BJBMB

Biobacta Journal of Biochemistry and Molecular Biology

https://bjbmb.org

SPBH

Review article

Flower-like nano- to micro-structured 3D functional materials: From conception to fabrication, application, and prospection

Jaafar Hasan[a, b], Dhurgham Aziz[a], Chuanguang Qin[b]*

[a]College of Dentistry, AL-Muthanna University, AL-Muthanna, AL-Samawah, 66001, Iraq.

[b]Shaanxi Key Laboratory of Polymer Science and Technology, OME Key Laboratory of Supernormal Material Physics and Chemistry, School of Chemistry and Chemical Engineering, Northwestern Polytechnical University, Xi'an, 710072, P. R. China.

Corresponding author: Jaafar.hassan84@mu.edu.iq

DOI: https://doi.org/10.71428/BJBMB.2026.0201

Abstract

Nanoflowers are an emerging class of flower-shaped nanoparticles that have attracted significant research interest because of their simple synthesis, excellent stability, and enhanced performance across a wide range of applications. This critical review provides a comprehensive overview of the advantages, limitations, synthesis strategies, classifications, and applications of nanoflowers from a future-oriented perspective, drawing on more than 200 research articles published since 2006. Owing to their unique three-dimensional morphology and high surface area, nanoflowers have demonstrated remarkable potential in targeted drug delivery, cell imaging, biosensing, protein functionalization, enhanced enzyme activity, improved stability, and catalytic processes. Their applications have further expanded to include enzyme purification, removal of dyes and heavy metals from wastewater, water splitting, fuel conversion, and energy storage technologies. Recent studies have also highlighted the use of three-dimensional nanoflower architectures to enhance surface sensitivity in Raman spectroscopy, enabling improved analytical performance. The exceptional surface-to-volume ratio and superior adsorption capacity provided by their petal-like structures make nanoflowers highly promising materials for next-generation technological applications. Furthermore, this review aims to provide valuable insights into the rational design and synthesis of advanced nanoflower-based photocatalysts, thereby supporting the development of sustainable technologies and inspiring future research in this rapidly evolving field.

Keywords: Nanoflowers, Controllable synthesis, Flower-like nanomaterial, Photocatalysis, Functional material

1. Introduction

Nanostructured materials have unique characteristics that can alter the anticipated pathways in biochemical functions [1]. Nanostructured materials of various forms have been produced thus far. For example, nanospear [2], nanoshells [3], core@shells [4, 5], nanoparticles [6, 7], nanoflakes [8], nanotubes [9], nanofibrils [10], nanosheets [11-13], nanorods [14, 15], nanoshales [16].

Nanoflowers (NFs) are flower-like nano/microparticles having nanoscale characteristics (e.g., petals) that may be used for catalysis [17], sensing, hydrogen production, water purification, and medication delivery, among other things [18-22]. A general method for preparing NFs

Received: April 4, 2026. Accepted: June 1, 2026. Published: August 8, 2026

is necessary for their technological uses. Their formation largely depends on serendipitous discovery and the simultaneous optimization of multiple synthesis parameters, including solvent selection, precursor concentration, and reaction temperature. The approach provided here bridges this gap, emphasizing the necessity of growing complex flower-like structures from a wide range of biomolecules.

“Nanoflowers” is a newly developed class of nanomaterials that shows a structure look like a flower. Recently, researchers used them for a particular group of nanostructures in a microscopic view [23, 24] and are gaining a lot of notice on account of their easy preparation, elevated stability, and increased activity. Among different nanoparticulate systems, nanoflower shows comparison to plant flowers in a nanoscale range between 100-500nm [25]. Nanoflowers have piqued researchers' interest due to their facile composition from organic or inorganic materials, and occasionally combining organic and inorganic elements to boost the surface reaction's stability and efficiency. Nanoflowers comprise numerous layers of petals (**Figure 1**) that combine to serve a more inclusive surface size in a tight structure that may be used for catalysis, biosensors, and drug delivery.

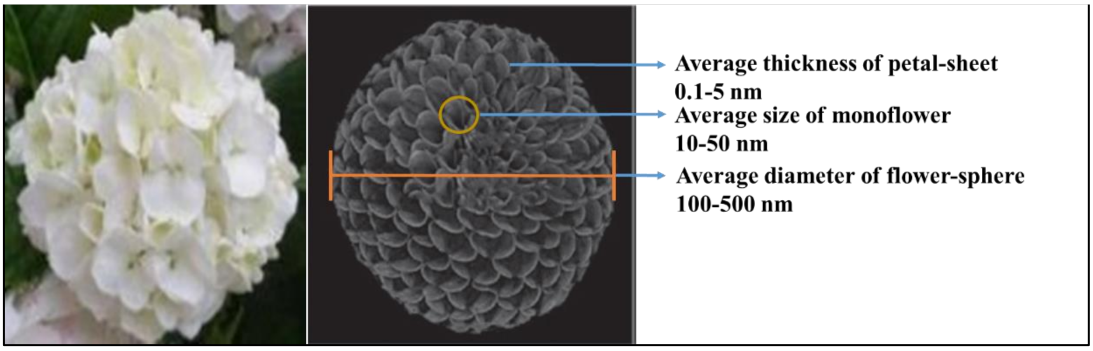

Figure 1. Structure of Nanoflower.

Although Nanoflowers are less well-known than nanowires or carbon nanotubes (CNTs), nanosheets, etc., depending on reaction conditions, different nanoflower structures were produced in the last decade, often in combination or equilibrium with other nanoforms. This mini-review covers the Current advances in the synthesis of nanoflowers for diverse groups of compounds: A state-of-the-art overview.

Nanoflowers showed excellent charge transfer and carrier immobility because of normous superficial area. The Ag-plated ZnO nanoflowers showed more excellent charge transfer and transporter immobility for surface-enhanced Raman spectroscopy sensitivity, which boosted the surface reaction's efficiency in the nanoflowers' three-dimensional structure [25].

Many scientists have worked to improve the structure and materials performance of nanoflowers and their composites. Ruixiang Yang and his co-authors prepared a novel flower-like $CuS/Bi_7O_9I_3$ as a catalyst via simple and mild reaction conditions. Ciprofloxacin (CIP) antibiotic was utilized to estimate the catalyst's degradation and sterilization performance. The results revealed a synergistic impact among the catalyst's photothermal and catalytic actions. The quick increase in temperature impeded the bacteria's biological function, disrupting their metabolism and speeding up the degradation of the composite catalyst [26].

A mild and green method manufactures a vacuum flower-like nanosphere heterostructure of carbon nitride and polydopamine ($g-C_3N_4$@PDA). This heterostructure efficiently prevents nanosheet agglomeration, allowing easier access to hollow nanospheres with a large specific surface area. Furthermore, during irradiation, the g-C_3N_4@PDA may effectively increase the production of ROS, leading to cell death and improving cancer therapy performance [27].

As for removing metals such as mercury and sulfur, some researchers, for example, Hui Zhang and his colleagues, reported that the bionic flower-like structure of g-C_3N_4/$Bi_4O_5I_2$ was easily synthesized using a one-step calcination technique. NB-1's mercury removal efficiency may be increased by 76%, greater than g-C_3N_4 and $Bi_4O_5I_2$. Electrochemistry indicates that the bionic structure helps to improve photocatalytic performance by facilitating migration efficiency and suppressing surface charge recombination [28]. Also, producing hollow flower-like NixZn$_2$-xV$_2$O$_7$/WO_4 composites using a sol-gel technique was described to improve the desulfurization efficiency of petroleum derivatives. SEM pictures revealed that all Ni, Zn, V, and elements W was involved in the product's synthesis; hollow flower-like nanostructures with a large superficial area were produced, although the shape was altered. The enhanced visible light absorption, good morphology, and high adsorption efficiency resulted in a photocatalytic oxidative desulfurization efficacy of more than 95% after 2.5 hours under visible light [29].

While Mousavi-Kamazani and his colleagues used Hierarchical flower-like AgI/Bi_2O_3 heterostructures by a glycothermal method, the results show that the photocatalyst with an energy bandgap (2.81 eV) has a high photocatalytic de-sulfurization efficiency of about 93% after 2 hr visible light irradiation, and also maintained stability after five recycles [30]. The flower-like $(Bi\,(Bi_2S_3)_9I_3)_{2/3}$ nanocomposites act as a good photocatalyst in the desulfurization [31].

In addition, Lifang Qi and his colleagues used a solvothermal technique to create hierarchical BiOIxBr (1-x) in the field of removing organic dyes, such as methyl orange (MO), Rhodamine B (RhB), bisphenol (BA), etc. Methyl orange (MO) as an objective pollutant was used under visible light irradiation to examine the photocatalytic performances of the as-prepared samples. Because of its hierarchical flower-like nanostructure, large specific surface area, and significant absorption of visible light, BiOIxBr(1-x) with a hierarchically spherical structure (the sample R75) was shown to have the maximum photocatalytic activity [32]. In other studies, solvothermal methods were used to make flower-like Dy^{3+}-doped Bi_2MoO_6, then as a photocatalyst to detoxify pollutants (RhB). The results exhibited good photocatalytic activity under simulated solar light irradiation. The RhB (10 mg/L) decay efficiency of 3 mol% Dy^{3+}-doped Bi_2MoO_6 was near 100% within 40 minutes, which was attributed to the photocatalyst's narrow bandgap energy (2.46 eV) [33].

A plain hydrothermal procedure was used to manufacture the heterojunctions of the flower-like g-C_3N_4/BiOBr combined as photocatalysts. The results explain that BiOBr-g-C_3N_4-4:1 showed perfect photocatalytic properties, and 96.6% of bisphenol (BPA) was removed in 120min with the illumination of visible light that was also because of its narrower bandgap than that of pure BiOBr [34].

3D flower-like MoS_2/rGO composites were synthesized via the hydrothermal method. The findings revealed that the MoS_2/rGO composite exhibited a large BET surface area, outstanding capacitive performance, and perfect capacitive deionization (CDI) with a maximum desalination capacity of 16.82 mg/g at 1.0 V in 200 mg/L NaCl solution. The composite's great desalination ability and electrochemical performance may be ascribed to its unique 3D flower-like MoS_2 structure haphazardly intertwined with rGO sheets and the synergies of rGO and 3D flower-like MoS_2[35].

In this review, the many forms of nanoflowers and their unique uses in the environmental field have been categorized to provide designers with information and guidelines (**Figure 2**). Based on previous research findings, we reviewed the general pros and drawbacks of nanoflowers and the present obstacles in nanoflower creation.

The progress related to the methods for synthesizing nanoflower materials, fabrication of nanomaterials, and formation of micro-/nano-structure materials is comprehensively reviewed and discussed in detail. This study seeks to highlight some of the advancements made by nanoflower materials in environmental applications and point the way for future research to bridge the gap between this type of material's realized and theoretical capabilities.

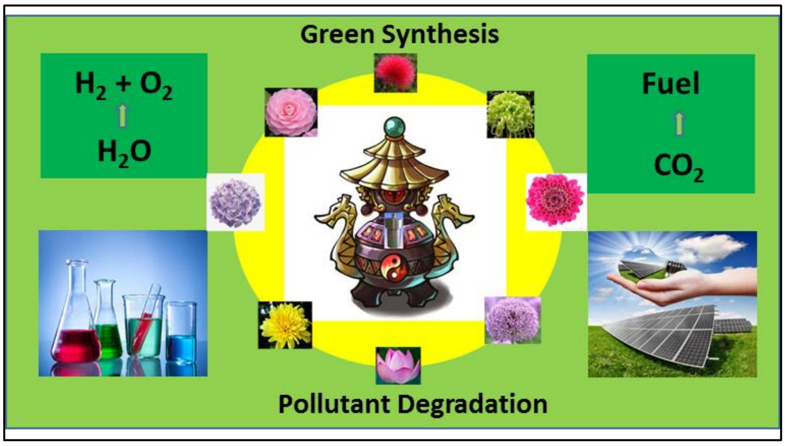

Figure 2. Schematic illustration of the formation of nanoflower-structure materials and the environmental applications.

2. Methodology of design and controllable synthesis

Scientists still desire advanced nanomaterials with unique structures and higher performance. So far, many methods such as High-temperature calcination, Hydrothermal, Solvothermal, Microwave-assisted synthesis, Green Antisolvent Method, Sol-gel method, Photo- or electro-deposition, and so on, have been used to prepare nano-materials with various structures like flowers. Nanoflowers are classified based on their size and design with metal ions [17, 36]. Nanoflowers are made from many atoms, such as cobalt, copper, molybdenum, nickel, etc, and their applications are mentioned in **Table** 1. More details on flower-like nano- to micro-structured 3D functional materials can be seen in **Table S1** as supporting information.

Table 1. Types of nanoflowers based on metal elements.

Component of a nanoflower	Metal element used for the synthesis	Morphology of 3D Structure	Application	Reference
cobalt phosphate	cobalt	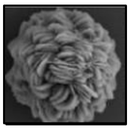	Increased enzyme activity and stability, increased catalysis, and improved nano-biocatalyst system construction.	[37]
Copper nanoflowers	Copper		The application can provide various medical diagnoses and biotechnology approaches, such as aptamers and peptides.	[38]
molybdenum disulphide	Molybdenum		To create solar hydrogen, particularly in the future, to provide a sustainable energy solution.	[39]
nickel hydroxide	nickel		The prospective application of a based supercapacitor in modern energy storage systems and electric cars is advantageous.	[40]
Cadmium sulfide	Cadmium		Application in the degradation of pollutants under visible light	[41]
Silver chloride	Silver		Provides a fresh view into the electrochemical process and the application area of visible light photocatalysts.	[42]
Manganese dioxide	Manganese		Long-cycle and quick-charge/slow-discharge supercapacitors for practical applications might be designed and manufactured using this simple synthetic technique.	[43]
Bismuth sulfide	Bismuth		This is used in a lithium-ion battery for the discharge capacity and charge.	[44]
Bismuth vanadate	Bismuth	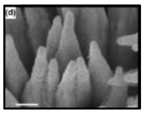	This work opens up a new pathway for oxygen deposition in artificial photosynthetic systems for water splitting.	[45]
Bismuth oxyhalides	Bismuth		They were used to successfully remove dye from aqueous solutions, utilizing more solar energy during water treatment under sunlight irradiation.	[46]

2.1 High-temperature calcination

Calcination is the warming (thermal treatment of) a solid chemical compound (e.g., carbonate ores) to elevate temperatures in the lack or tied supply of air or oxygen (O_2), generally to remove imperfections or volatile substances and to afford thermal decomposition or thermal processing (of a catalyst) in an oxidizing atmosphere. The calcination temperature is generally slightly higher than the operating temperature of the catalyst. Various types of nanoflowers have been successfully synthesized via the thermal calcination process. The study of calcination in aqueous solutions and the preparation of pure oxide powders by this method are still in their early stage [47-49].

For example, to manufacture the porous 3D flower-like Co/CoO, a flexible and straightforward two-step technique, including hydrothermal and subsequent annealing procedures, has been devised [50]. It is noted that the appropriate heat treatment influenced the flower-like structure, composition, and electromagnetic absorption characteristics of the material, as shown in **Figure 3**. In particular, the porous 3D floral design can only be obtained at 400 °C. When the safeguard temperature reaches 300 °C, the Co element cannot be produced. Furthermore, when the annealing temperature was raised from 400 to 500 °C, the flower-like nanostructures could no longer be retained because the larger porosity diameter would destroy the floral frame.

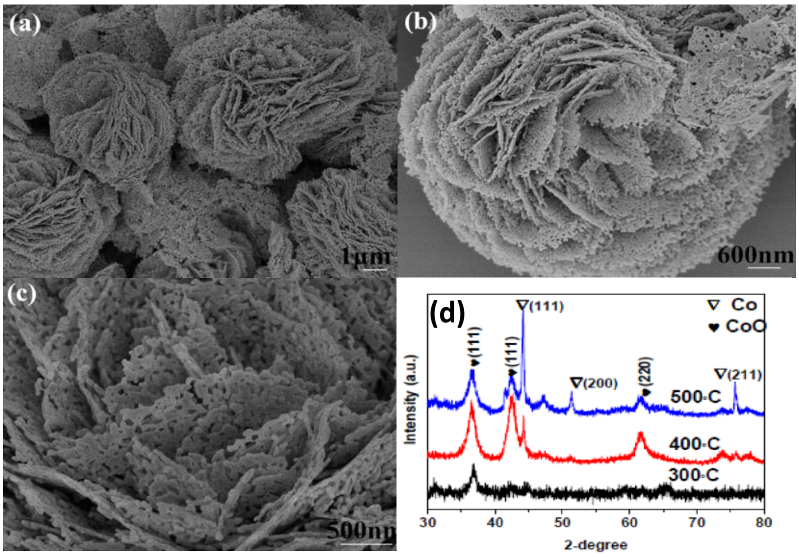

Figure 3. The SEM images (a-c) of the 3-D flower-like Co/CoO (prepared at 400 °C), (d) The XRD patterns of the Co/CoO prepared at 300-500 °C. Reprinted with permission [50] Copyright 2015, ACS

2.2 Hydrothermal Synthesis

Among the most often utilized techniques for nanoflower production is hydrothermal synthesis (solution reaction-based method). Nanoflower formation could occur in wide temperature ranges during hydrothermal synthesis, from room to extremely high temperatures. High- or low-pressure conditions might be utilized to control the materials‘ morphology to be manufactured based on the vapor pressure of the fundamental structure in the reaction. A wide range of nanoflowers has been efficiently synthesized using such a method. The hydrothermal synthesis approach has several benefits compared to others. Nanoflower might be produced through hydrothermal synthesis. while it is unstable at high temperatures. The hydrothermal process could make a nanoflower with minimal material loss and high vapor pressures. In hydrothermal synthesis, the compositions related to the nanoflower to be synthesized might be excellently controlled using a multiphase or liquid-phase chemical reaction [51]. See **Figure 4,** which shows the hydrothermal process.

For example, the hydrothermal technique was used under various conditions to produce a rod, such as a tetragonal ε-MnO_2 flower, such as hexagonal magnet. The structure of the ε-MnO_2 sample was obtained by water-bathing with $KMnO_4$ and a copper plate as the metal source. The sequence α-$MnNO_2$ > ε-$MnomO_2$ > β-$MnnO_2$ reduced the descent-temperature reducibility and oxygen form concentration. 90 % toluene conversion temperatures over the three materials were 238, 229, and 241 °C at 20,000mL/ (g h) space velocity. The obtained results presented that the superior capacity of the materials resulted from the reproduced oxygen concentrations and low-temperature synthesis [52]. **Figure 5** shows the SEM and TEM morphological images of the rod-like tetragonal and flower-like hexagonal magnet

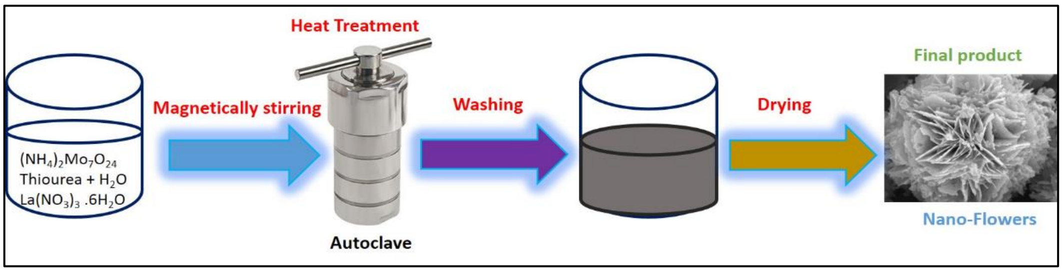

Figure 4. Hydrothermal synthesis method

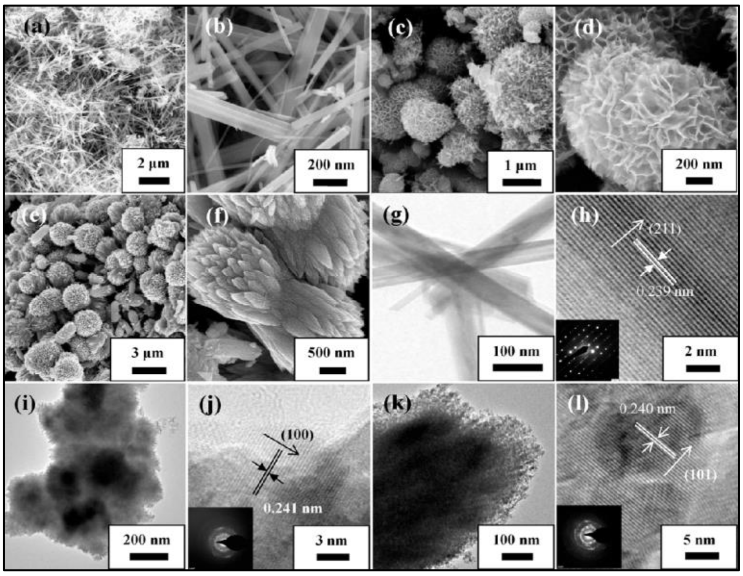

.

Figure 5. (a-f) SEM images and (g-l) TEM images and the SAED patterns (insets) of (a, b, g, and h) rod-like α -MnO_2, (c, d, i, and j) flower-like ε -MnO_2, and (e, f, k, and l) dumbbell-like β -MnO_2. Reprinted with permission [52]. Copyright 2012, Elsevier

2.3 Solvothermal Synthesis

One of the most common methods for preparing materials on the micro and nanoscale is the Solvothermal process. This synthetic method has several advantages, including ease of use, cost savings, and the ability to regulate the size and shape of materials. Solvothermal synthesis is a chemical reaction in a solvent at a temperature higher than the solvent's boiling temperature in a tight vessel. This procedure provides accurate control over the particle size and shape distribution by modifying the reaction parameters. As illustrated in **Figure 6a**, this procedure is usually completed in a tight tank known as an autoclave, built of steel or another strong alloy, and can withstand the pressure it makes during the reaction. The autoclave has a Teflon lining that prevents corrosion and provides a chemically inert vessel for the chemical reaction.

Nanoflowers with various shapes and sizes have been obtained through Solvothermal reactions combined with a post-calcination process. For example, XuefengLiu and his colleagues reported 3D black N-TiO_2-x@MoS_2 core-shell nanostructures synthesized by hydrothermal reaction and a chemical reduction method, pursued to 350 °C calcination under an argon atmosphere **Figure 6b**. The findings indicated that the core-shell heterojunction nanostructure formed by the 3D N-TiO_2-x@MoS_2 photocatalyst is effectively doped with N and Ti^{3+} while concurrently coupling with MoS_2. The N and Ti^{3+} co-doped and hybrid heterostructures can efficiently decompose methyl orange and generate hydrogen using visible light and solar energy. The rates of methyl orange decomposition and hydrogen generation are 91.8 % and 1.882 mmol $h^{-1}g^{-1}$, respectively[53].

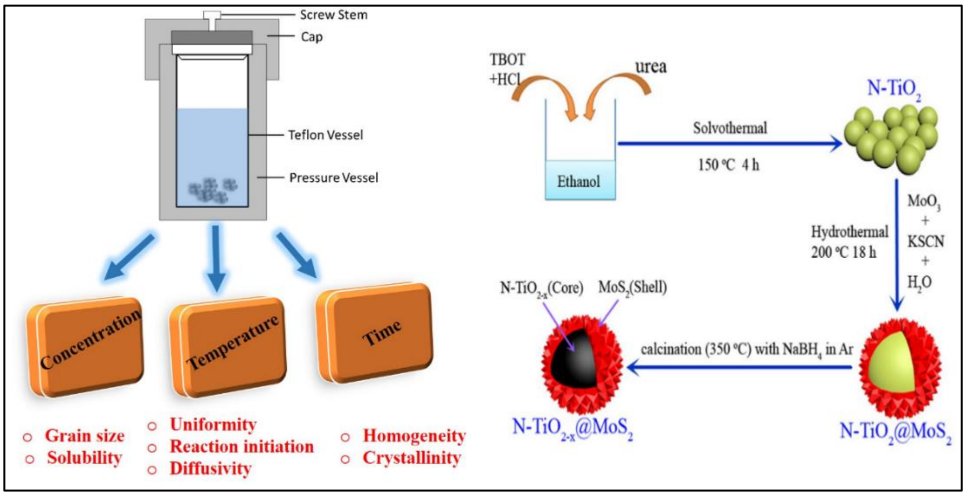

Figure 6. (a) Schematic of autoclave Teflon liner used in the solvothermal method, (b) The schematic as-synthesis of the N-TiO_2-x@MoS_2 nano-composites. Reprinted with permission [53]. Copyright 2017, Elsevier

2.4 Microwave-assisted synthesis

Microwave (MW) chemistry in synthetic organic chemistry has increased reaction rates, product yields, and selectivity [54]. The method can synthesize high-quality nanoflowers by heating the molecular precursors directly using MW. Also, the MW-assisted route was used for one-step synthesis regarding a wide range of mono- and bimetallic nanostructures. Typically, the synthesis involves the reduction of metal salts in aqueous media in the presence or absence of surface-directing agents or organic solvents like ethanol, methanol, polyols, and so on [55]. Ionic liquids were also employed to produce metal nanostructures because of their polarizability and high ionic conductivity, making them effective MW-absorbing agents. Metallic nanostructures of varied morphologies and sizes were created by varying the precursor concentration, precursor, solvent, and industrial parameters such as MW power, temperature, and pressure. The MW-assisted route has also been utilized to synthesize a set of complex and straightforward metal oxides. A wide range of ternary and binary oxides was prepared using the MW-hydrothermal technique. Furthermore, organic solvents, like benzyl alcohol or ethylene glycol, are ideal alternatives to the aqueous systems because of their dielectric loss factors and high boiling points, alongside the certainty that they combine all of the advantages of nonhydrolytic/nonaqueous NP synthesis with MW chemistry.

Juliana S. Souza and colleagues [56] found that MW-irradiated Au-BiVO4NF showed comparable physical-chemical properties to those made out of traditional heating. Yet, the time needed for synthesizing the heterojunction has decreased from 4 hours to 10 minutes. Since BiVO4 has a low band-gap energy and AuNPs might operate as electron sources or as electron sinks via plasmon resonance, the heterojunction is considered one of the very significant photocatalysts under visible light irradiation, increasing the charge separation related to photo-generated holes and electrons. After 6 hours of UV-visible light irradiation, the synergic impact of the heterojunction led to a 95% breakdown of methylene blue. In addition, Figure 5 exhibits TEM images regarding the heterojunction created between AuNP and $BiVO_4$ throughout the materials synthesis utilizing conventional and MW heating. Using MW irradiation as one of the heating sources, irregular structures have been acquired with molar ratios of 1:1 (a), 1:5 (b), and 5:1 (c) of (Au: Bi) (**Figure 7**a, b, and c, respectively).

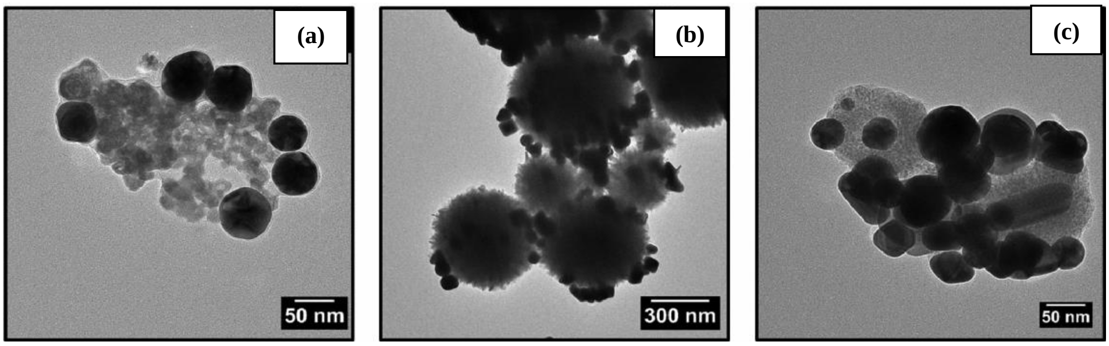

Figure 7. TEM images of Au: Bi molar ratio at 1:1 (a), 1:5 (b), and 5:1 (c) of (Au: Bi). Reprinted with permission [56]. Copyright 2019, Springer

In the synthesis of inorganic nanomaterials, MW radiation has proven to be a very efficient heating source. It has the following benefits: an effective heating source (super-heating) resulting in an increase in the reaction rates, allowing more rapid synthesis, size, and shape control, more chemical reaction reproducibility in comparison to traditional heating, selective MW heating, and likely MW chemistry combinations [57].

However, MW dielectric heating has drawbacks, including restricted applicability, safety, scalability, and health risks associated with the MW-heating apparatus [57].

2.5 Green Antisolvent Method

The three major essential parameters for the nanomaterials' synthesis are selecting a suitable reducing agent, an environmentally friendly solvent, and a safe material for stabilization. Extensive synthetic routes were used for synthesizing nanoflowers, with chemical, physical, and biosynthetic pathways being the most frequent. Chemical procedures are typically costly and include toxic and hazardous chemicals that pose various environmental hazards [58]. The biosynthetic path, however, is a biocompatible, safe, and environmentally friendly green approach for synthesizing nanomaterials for biomedical purposes utilizing microorganisms and plants [59]. Algae, fungi, plants, and bacteria, among various applications, might be utilized for carrying out such synthesis. Plant parts, like fruits, leaves, stems, roots, and seeds, were utilized to synthesize various NPs due to phytochemicals in their extract, which function as a reducing agent and a stabilizer [60].

Ji-Yao Dong and colleagues prepared single-crystalline mesoporous ZnO nanosheets in the shape of flowers using a solvent-based antisolvent method followed by calcination at 300 °C. The antisolvent approach resulted in the production of zinc carbonate hydroxide and zinc oxide nanosheets. The as-produced nanosheets were ultrathin, with a thickness of about 10 nm and pore diameters ranging from 10 nm to several tens of nanometers as the calcination time and temperature increased (**Figure 8**), where the antisolvent process's as-prepared product was randomly stacked together. These nanosheets, like a flower, showed excellent photocatalytic efficiencies comparable to those of a commercial photocatalyst, P25, regarding photocatalytic degradation of a model pollutant, like methylene blue. The high photoactivity attained in the degradation of methylene blue was attributed to the structural advantages of the nanosheets of being ultrathin, mesoporous, and single-crystalline [61].

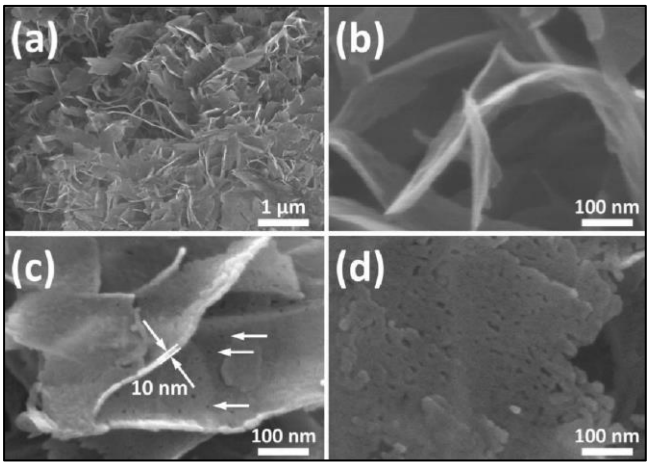

Figure 8. The SEM images show as-designed samples at low-magnification(a) and high magnification (b), as well as models, calcined at 300 °C for 30 min(c) and five hr.(d). Reprinted with permission [61]. Copyright 2012, RSC.

2.6 Sol-gel Method

Sol-gel is a high-controllability, low-temperature, inexpensive technology for producing highly stoichiometric, homogeneous, and high-quality ultrafine nanostructure materials. Also, this approach allows you to customize the nanostructure's shape [62]. The sol-gel route makes flower-like NPs since it is a cost-effective, simple, and industrially viable approach that creates a high-quality coating. In addition, it can sinter at low temperatures and shape materials into complicated geometries while in a gel state. Those advantages make the sol-gel technique of production especially appealing [63, 64]. The schematic diagram related to the sol-gel process is shown in **Figure 9a**. Furthermore, the experimental setup is straightforward. Sol is made by adding appropriate reagents to a precursor solution and performing polymerization or hydrolysis.

Anshika Nagar and co-authors reported that Zinc Oxide nanoflowers/nanoparticles were synthesized via the sol-gel method. Zinc acetate and distilled water were utilized in the synthesis. **Figure 9b** shows the nanoflower-like structure of zinc oxide nanoparticles revealed by FESEM morphological analysis. Furthermore, the as-grown ZnO nanoflowers demonstrated a high current density of 30.5 mA/cm^2, a low turn-on field at 1.2 Vμm-1, and a good field enhancement factor. The findings open the door to a more controlled, diverse, and simple way of preparing ZnO nanoparticles for display device research [65]. In addition, for the first time, K. Haouemi and his colleagues reported TiO_2 nanoflowers by the sol-gel technique inside a reverse microemulsion. Scanning Electron Microscopy (SEM) revealed that the material comprises belt-shaped particles that convert to a nanoflower morphology after being heated to 600 °C. A suggested model might explain the growth process from nanobelt to nanoflower. As shown in **Figure 9c**, each flower comprises multiple nano petals linked to form 3D nanoflowers [66].

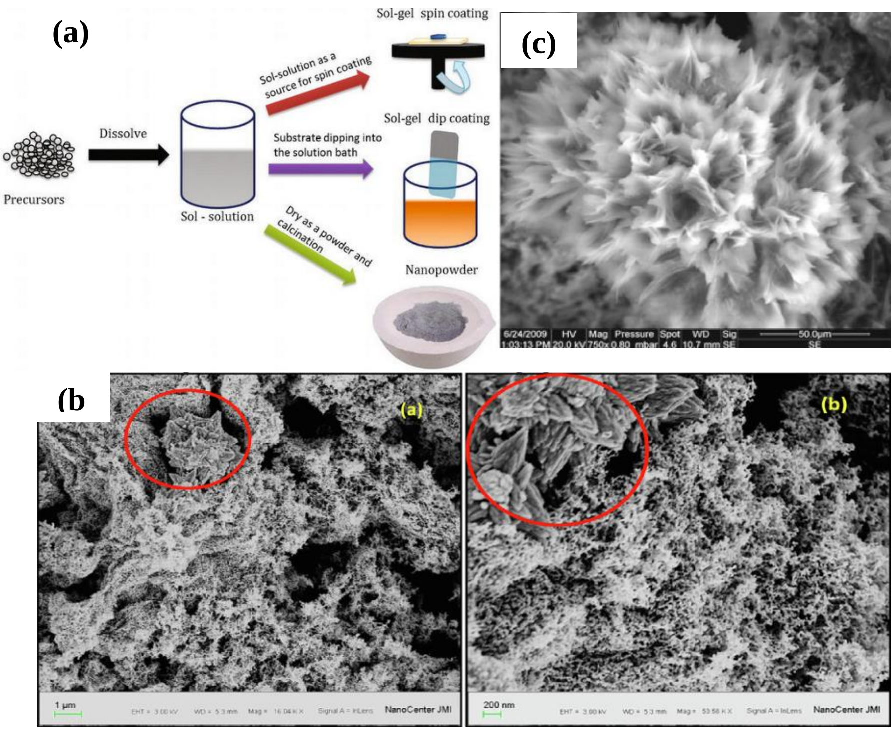

Figure 9. (a) Schematic diagram of sol-gel processing, (b) FESEM micrograph of the nanoflower-like structure of zinc oxide nanoparticles. Reprinted with permission [65]. Copyright 2020, Elsevier, and (c) SEM image of a single nanoflower.

2.7 Electrodeposition Method

Electrodeposition is a versatile and low-cost way of fabricating two- and three-dimensional materials, including coatings and films. Electrochemical processes linked with the reduction or deposition of electroactive and accompanying species on the cathode surface are the basis for the electrodeposition process. A more precise electrodeposition method can be achieved by utilizing electrochemical principles for specific objectives and applications [67]. In addition, as compared to the hydrothermal technique, this method has several benefits, including high safety, a low processing temperature, a quick precipitation time, and a waste-minimized material [68].

P. Dhanasekaran and his colleagues [69] reported that 3D-dimensional ultra-fine platinum nanoflowers are directly deposited on a carbon-coated gas diffusion layer electrode (C-GDL) by a single-step electrodeposition method towards the application of polymer electrolyte fuel cells. Notably, the Pt nanospheres convert into a 3D nano-flower with increased current density from (-1.6 to -32 mA cm^{-2}). A steady-state polarisation study used an electrodeposited Pt catalyst on C-GDL as the cathode catalyst. Among the electrocatalysts developed, the nanoflower-shaped Pt catalyst has a high peak power density of 660 mW $cm-^{2}$ at 0.6 V in polytetrafluoroethylene. **Figure 10a** shows the surface morphology of C-GDL after electrochemical deposition of Pt metal nanoparticles.

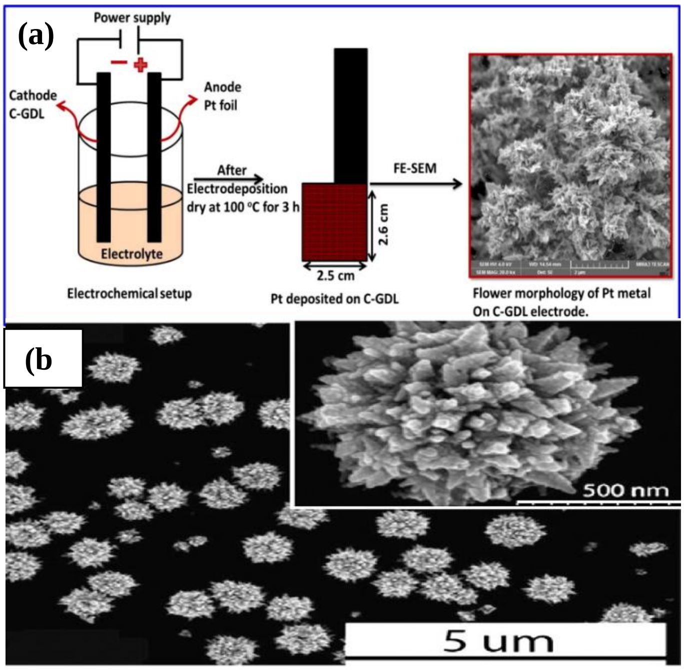

Figure 10 (a) Schematic diagram of Pt metal nanoparticles deposited on carbon-coated GDL and its surface morphology. Reprinted with permission [69]. Copyright 2020, Elsevier and (b) SEM images of Pt catalysts electrodeposited with Pt nanoflowers. Reprinted with permission [70]. Copyright 2010, Elsevier

In another study, Hongmei Zhang and his colleagues reported a facile, single-step electrodeposition method for the first time to produce porous Pt nanoflowers for applications in energy and catalysis. The flower-like architectures were confirmed by SEM analyses, as shown in **Figure 10b**. In contrast to conventional nano-sized Pt catalysts, the as-prepared Pt nanoflowers exhibited remarkably more catalytic activity and more robust toxicity tolerance for the methanol electro-oxidation[70].

Juan Zhou et al. reported the synthesis of sensitive H_2O_2 biosensors via electrochemical precipitation of Au-Pt bimetallic nanoparticles (NPs) on molybdenum disulfide nanoflowers (MoS_2 NFs). The results showed that MoS_2-Au/Pt nanocomposites exhibited perfect catalytic efficiency for specific detection of H_2O_2, together with high enzyme-free electrochemical sensor ability in a linear range of 10 µM to 19.07 mM with increased sensitivity of 142.68 µA mM^{-1} cm^{-2}[71]. In addition, Au-Pt bimetallic flower nanostructures on a polyamidoamine dendrimers-modified surface were also made via electrodeposition. The AuPt bimetallic nanoflowers remained stable during the electrodeposition process, and the average size of the nanoflowers increased with the rise in electrodeposition time[72].

Various flower-like, for example, SnO_2 sensor Flower-like, nano-ZnO flower-like, Fe_3O_4 nanostructured flower-like, 3D mesoporous Ce-ZnO flower-like, etc., are discussed in **Table** 2 concerning their different synthetic methods and functions.

3. Morphology characterization of nanoflowers

Characterization is an essential field in material science. It is assigned to describe the physical and chemical properties of the material for a better understanding. The material's performance may be optimized using this high degree of information. In Nano flowers, characterization techniques are widely utilized to prove the quality and the purity of the produced Nano flowers. Moreover, Characterization methods are beneficial for deciphering the nano-flower performance and analyzing the composition. (Table 3)

4. Chemophysical analysis and photoelectrochemical performance

4.1 X-Ray Photoelectron Spectroscopy

Siegbahn and colleagues created the surface analysis technique (SCA) in the 1960s to examine materials' chemistry and qualitative atomic composition [111]. XPS could be utilized for detecting the binding state/energy values regarding substances, and variations in binding state/energy levels may be used to determine an element's chemical state. The XPS principle states that a flat sample or specimen is bombarded with well-defined X-rays, which react with inner electrons around the nucleus [112]. Furthermore, electrons will be emitted at well-defined kinetic energy, which EK has represented in the equation below [113]:

$$E_K = h_v - E_b - \phi, \qquad (1)$$

In which h_v represents the irradiated X-ray photon energy, ϕ represents the sample’s work function, and E_b indicates electron binding energy. From the eq., it could be suggested that kinetic and binding energy levels regarding emitted electrons depend on irradiated photon energy on the sample’s surface. Also, the photo-electron spectrum showing the chemical state, elemental identity, and detected element quantity has been listed by calculating the removed electrons over a range of electron kinetic energy values [114].

Table 2. Methods for the synthesis of Flower-like nanostructure and their function.

Flower-like	Method of synthesis	Function	Reference
SnO_2 sensor Flower-like	Method: prism-like, a blend of nanoflowers, a simple surfactant-assisted route in hydrothermal	The enhanced sensor response of these sensors	[73]
nano-ZnO flower-like	Without ultrasonic treatment, hydrothermally synthesized materials with or without ultrasonic aid have more extensive oxygen vacancies and display more evident green emissions.	Suppressing green emissions and reducing the photocatalytic activity of such flower-like ZnO.	[74]
Fe_3O_4 nanostructured flower-like	The solvothermal method to synthesize large-scale 3D flower-like iron oxide precursors, Anhydrous ($FeCl_3$), is used as the iron source.	As an optical probe with magnetic function for application in high-sensitivity bioassays.	[75]
3D mesoporous Ce-ZnO flower-like	The one-step wet chemical method at room temperature: a facile method to synthesize Ce-doped mesoporous 3D flower-like ZnO at room temperature.	Remove the organic pollutants RhB and phenol for water purification.	[76]
3D Micro/Nano Ce−Mo flower-like	Synthesized through an ethylene−glycol−mediated process: samples were first evaluated as catalysts in the reactions of HMF to DFF and fructose to HMF.	I am using it in the industrial production of Diformylfuran (DFF) from fructose.	[77]
Au-BiOI nanohybrids flower-like	A facile wet chemical method: where gold nanoparticles (~15 nm) are uniformly decorated on the surface of 3D flower-like BiOI microspheres.	a promising candidate for Environmental remediation.	[78]
BiOI/MoS_2 heterostructures flower-like	A facile hydrothermal method: BiOI nanoplates grew on the surface of exfoliated MoS_2 nanosheets.	Application of photocatalysts in environmental purification, marine antifouling, and energy conversion.	[79]
$BiVO_4$/ BiOI core/shell heterostructure flower-like	A simple hydrothermal method: depositing BiOI irregular nanosheets on the surface of sphere-like $BiVO_4$ particles via an in situ precipitation method	Photocatalytic performance and adsorption capability for the removal of antibiotic pollutants.	[80]
Gold nano chains, flower-like	A one-step synthesis with the assistance of caffeine as a structure-directing and weak stabilizing agent.	Applications in the construction of optical and catalytic devices.	[81]
MoS_2-PEG nanoflakes flower-like	a simple hydrothermal method and synthesized the LA-PEG polymer onto their surface to construct the MoS_2-PEG nanoflakes	As promising photothermal agents for future photothermal cancer therapy.	[82]
CoS-decorated 3D porous carbon Skeleton flower-like	One step of the solvothermal synthesis process was applied in the detection of glucose with excellent analytical performance	promising for the international trend of eco-friendly environmental production, especially in the blood or food industry.	[83]
Zinc oxide (ZnO) nanoflowers	Through zinc (II) nitrate and ammonia by a domestic microwave (MW) oven.	a therapeutic agent for cardiovascular diseases	[84]
flower-like $NiWO_4$/WO_3 heterostructures	solvothermal and hydrothermal methods, and subsequently utilized in gas sensors for TMA detection	a highly promising sensing material for TMA gas sensors.	[85]

Table 3. Parameters for morphology characterization of nanoflowers

Parameter	Use	Reference
Optical microscopy	To get the best resolution images to investigate the morphology	[86, 87]
Scanning Electron Microscopy (SEM)	used to survey the size and surface morphology	[88-92]
Transmission Electron Microscopy (TEM)	To determine the internal structure to provide the nanomaterial's morphological and structural components and crystallographic data.	[93-95]
Atomic force microscopy (AFM)	To offer three-dimensional topographical images with higher resolutions. To study surface properties.	[96-98]
X-ray diffraction (XRD)	To study the surface properties of the structural composition of nanomaterials.	[99-103]
Thermogravimetric analysis (TGA)	To measure the change in the weight of the nanomaterial that is dependent on temperature and time	[104, 105]
Energy Dispersive X-Ray Spectroscopy (EDX)	To perform elemental analysis for nanomaterials	[106, 107]
Zeta size and zeta potential	To determine the particle size and stability of a colloidal dispersion	[108]
FTIR spectroscopy	To identify the drug by functional group	[109, 110]

4.2 Distribution of UV reflectance spectra

UV/vis spectroscopy can be defined as a spectroscopy type that utilizes electromagnetic radiation with wavelengths in the range of (190-800) nm, depending on the analyte's reflection, absorption, scattering, diffraction, and refraction characteristics [115]. Also, electromagnetic radiation is classified into two regions: (400-800) nm and (190-400) nm, which correspond to visible and UV, respectively [116]. The light absorption creates a difference in the electronic energy levels in the material throughout the analysis, which is why it's also known as electronic transition spectroscopy [117]. Also, the electron's transfer through the bonding orbital to the anti-bonding orbital causes a shift in energy levels [118]. Light from the source, commonly a mercury lamp or xenon arch, reacts with the sample in principle (contained in the cuvette). The sample exhibits light absorption, and valence electrons are excited. The detector records the model/blank intensity ratio [104]. Transmittance T is considered the ratio of the powers recorded through the detector and is determined by the equation below [119]:

$$T = \frac{I}{I_0} \qquad (2)$$

I represent transmitted intensity, and I_0 represents the original/ reference intensity. The following equation might be used to relate absorbance A and transmittance:

$$A = -\log T \qquad (3)$$

UV-vis spectroscopy is fundamentally based on Beer–Lambert's law, which indicates that the absorption of incident light is directly proportional to the concentration of absorbing molecules in a solution. Equation (8) of Beer–Lambert's law can be represented as:

$$A = \varepsilon c l, \qquad (4)$$

In this context, ε denotes the molar extinction coefficient expressed in dm^3/mol•cm, c signifies the concentration of the absorbing species measured in mol/dm^3, and l refers to the optical path length of the glass cuvette, measured in centimeters.

As has been previously stated, various transitions occur in the case when a sample interacts with incident light. Most significant shift is from the low energy orbital, which has been known as HOMO (i.e., highest occupied molecular orbital), in which unexcited electrons might be identified, to the maximum energy orbital, which is known as LUMO (i.e., lowest unoccupied molecular orbital) [120].

The d-d transition between ligand-to-metal-charge transition and metal ions are two possible transition for flower-like nanomaterials. Because nanocomposites contain both inorganic and organic materials, their UV spectra may have transitioned between the two. UV/vis could be utillized to analyze nanomaterials‘ band gaps, semiconductors, and nano-composites with semiconductor characteristics and electronic transitions. Furthermore, many shifts could be used to observe the effective nanocomposites' preparation. These shifts include (1) red shifting or bathochromic (i.e., the shifting toward more extended wavelength), (2) Auxochrome (substituents that don't absorb light yet shift the maxima of the absorption to longer wavelengths), (3) hypochromic effect (reduces absorption intensity), (4) blue shift or hypsochromic (a shift toward shorter wave-length), and (5) hyperchromic effect (causes an increase in the absorption intensity) [120].

4.3 Gas adsorption-desorption isotherm

The gas adsorption approach is a popular way to determine a material's pore size distribution and specific surface area. The principle is dependent on the property of gas absorption on solid surfaces. Under particular pressure, the equilibrium adsorption capacity has been evaluated; a theoretical model has acquired the pore size distribution, specific surface area, and amount of physical adsorption in a tested sample [121].

Nitrogen adsorption is a common technique for determining materials' pore size distribution and specific surface area at low temperatures. Nitrogen-relative pressure (P/P0), in which P represents the nitrogen's partial pressure and P0 means nitrogen's saturated vapor pressure at liquid nitrogen temperature, determines the nitrogen's surface adsorption capacity on a solid surface. Adsorption and relative pressure P/P0 fit Brunauer, Emmett, and Teller's (BET) equations when P/P0 ranges between 0.05 and 0.35. The nitrogen adsorption approach uses this as the foundation for determining specific surface areas. Capillary condensation causes nitrogen to condense in the micropores when P/P0 equals or exceeds 0.4. Theoretical analysis and experimentation could select the pore volume and size. MW-treated wood could be analyzed using mercury intrusion porosimetry; the microscopic pore structure in large pore sizes ranges between (2 and 400,000) nm; however, this approach is more precise in macro-pore analysis (>50 nm). Furthermore, the nitrogen adsorption technique might be used to analyze the concentration analysis related to pore structures with smaller pore sizes, as well as the accurate analysis regarding material macropores (50 nm) and mesopores (2-50 nm) [121].

4.4 Raman spectroscopy

Raman spectroscopy serves as a non-destructive method for chemical analysis, providing insights into the chemical structure, phase, and polymorphic forms, crystallinity, and molecular interactions. This technique is centered on how light interacts with the chemical bonds of a substance. A Raman spectrum, characterized by multiple peaks, illustrates the intensity and wavelength position of the scattered Raman light, as demonstrated in Figure 11. Each peak corresponds to a distinct chemical bond vibration, such as C-C, N-O, C-H, etc.

In addition, we have summarized the applications of nanoflowers in published papers from 2006 to 2025 by more than 200 relevant key literature, as shown in **Figure 12**.

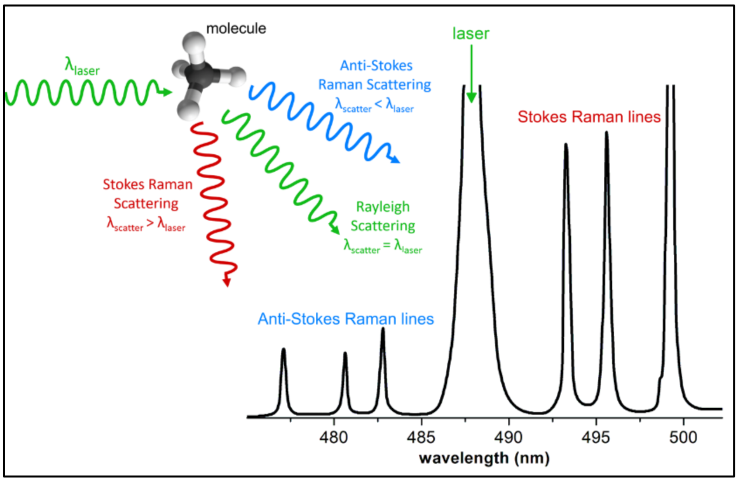

Figure 11. The emission Raman scattered light.

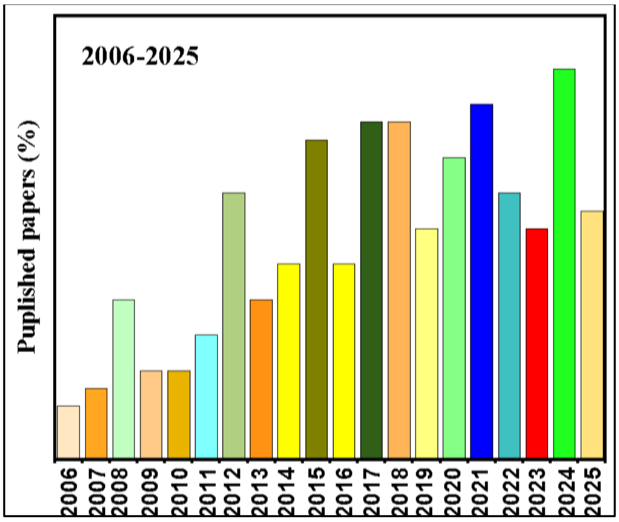

Figure 12. They summarized the applications of nanoflowers in published papers from 2006 to 2021.

5. Applications of nanoflower

Nano-flowers applications are critical in everyday life; there are several applications in the field of nano-flowers, which we have briefly discussed and have included in various fields. Applications of nanoflowers in different areas are shown in **Figure 13**.

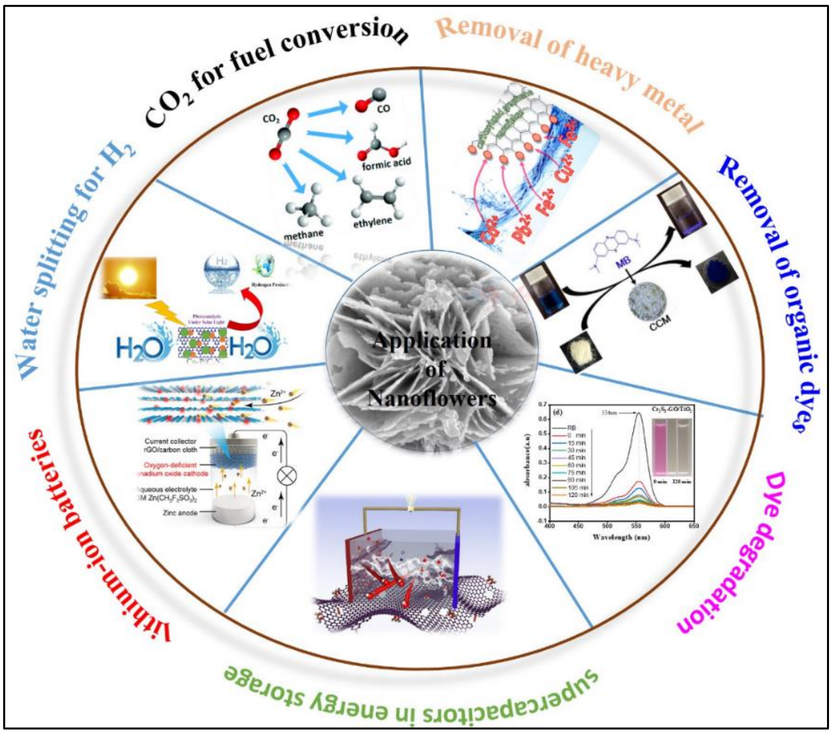

Figure 13. Applications of nanoflowers

5.1 Water splitting for H_2 production

Hydrogen stands out as a renewable and sustainable energy source, promising to address the challenges posed by traditional fossil fuels, such as energy shortages and pollution. It has long been identified as a leading candidate for tackling the global energy crisis and environmental damage. The processes of photocatalytic hydrogen (H_2) evolution using solar energy and the electrochemical hydrogen evolution reaction (HER) through water splitting have captured the interest of researchers worldwide. Numerous catalytic systems have been developed, combining a light-harvesting photocatalyst made from abundant materials with a co-catalyst that is electrically conductive, often involving noble metals. Water splitting, which includes the evolution of hydrogen at the cathode and oxygen at the anode, offers an effective means of producing both hydrogen and oxygen. To achieve widespread hydrogen production necessary to meet future energy needs, efficient solar light-driven water splitting is crucial. When exposed to sunlight, water (H_2O) breaks down into hydrogen (H_2) and oxygen (O_2) molecules [122-124], as illustrated in Figure 14.

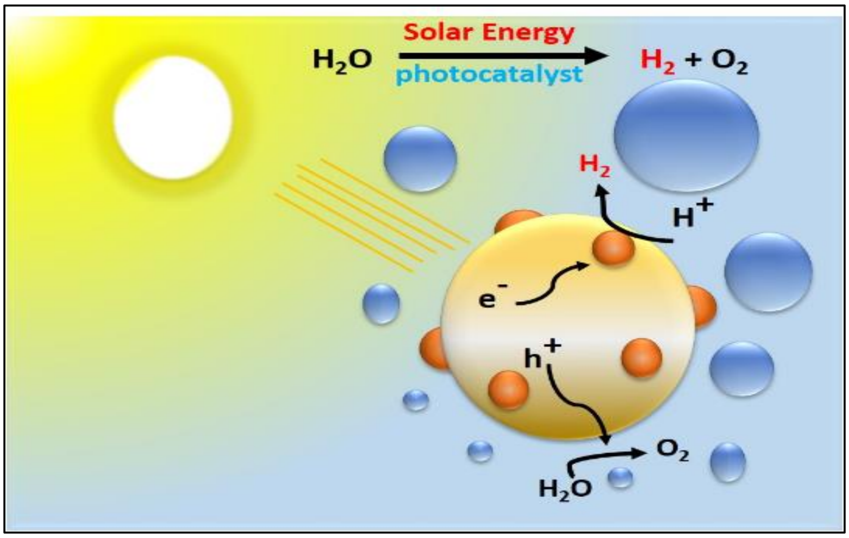

Figure 14. The photocatalysis process for hydrogen production

In recent years, innovative nanoflower heterostructured nanocomposites have been effectively utilized as proficient photocatalysts to enhance the photocatalytic production of hydrogen.

For instance, Ranjit Bariki et al. reported a novel UiO-66/$CdIn_2S_4$ heterojunction nano-composite via a hydrothermal method [125]. A hierarchical 3D micro flower structure with improved surface reactive sites was discovered after extensively evaluating the UiO-66/$CdIn_2S_4$ nanocomposites. The photocatalyst 30UiO-66/$CdIn_2S_4$ showed a higher H_2 evolution rate (2.95 mmol g^{-1} h^{-1}), with an apparent quantum efficiency of 20.8 %. Herein, the water-splitting reaction was carried out with a sacrificial agent of 10% methanol to collect the holes generated throughout the response. The visible-light photocatalytic H_2 generation rate of CIS, UiO-66, and (X) UiO-66/CIS nanocomposites are shown in (**Figures 15**a & b). Pure $CdIn_2S_4$ (CIS) exhibited a photocatalytic H_2 evolution rate of 0.21 mmol g^{-1} h^{-1} when subjected to the same reaction conditions as the nanocomposites. When the amount of UiO-66 in an (X) UiO-66/CIS nanocomposite increases to 30%, the rate of H_2 evolution increases to 2.95 mmol g^{-1} h^{-1}. The most significant rate of H_2 generation is seen in the 30UiO-66/CIS nanocomposite, which is approximately 14 times that of pure $CdIn_2S_4$.

For photocatalytic H_2 generation, the recyclability and stability of the 30UiO-66/CIS photocatalyst are investigated for up to four consecutive cycles (**Fig**ure 15c). Under visible light irradiation, a minor reduction of 3% H_2 generation is seen after the fourth photocatalytic cycle. No discernible change in crystalline structure or shape suggests that the 30UiO-66/CIS photocatalyst is highly stable in the H_2 generation.

Moreover, the study conducted by Khalid Nadeem Riaz and colleagues documented (3D) flower-like MoS_2 nanostructures prepared via the hydrothermal method by varying temperatures and reaction times. According to the findings, the best sample, produced at 200°C for 24 hours, had a 3D flowerlike MoS_2 nanostructure. It is widely recognized that the photocatalyst's surface area, composition, and shape significantly impact its photocatalytic activity [126]. Furthermore, the lanthanum element (La^{3+}) was used to modify this new photocatalyst using different La^{3+} atomic ratios. Under the same conditions, the flower-like

3% $LaMoS_2$ nanostructure photocatalyst exhibited a 5.2-fold increase in efficiency for hydrogen evolution during water splitting compared to pure MoS_2. It produced a total of 110 mol/h of hydrogen over six hours of visible light exposure, as illustrated in Figure 16 (a & b). Lanthanum doping, which enhances photogenerated charge carrier transfer and extends electron lifetime, may be responsible for the remarkable photocatalytic activity in this nanocomposite [127, 128]. This research provides a low-cost photocatalyst for water-splitting energy generation [129].

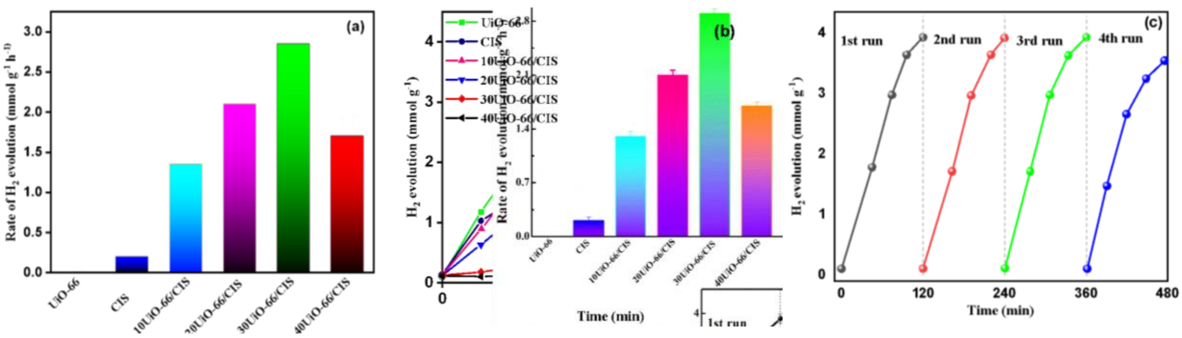

Figure 15. (a) Photocatalytic H_2 evolution rate caused by visible light, (b) amount of H_2 generation wrt. of UiO-66/CIS nanocomposites together with pure CIS and UiO-66, and (c) reusability test for four cycles of photocatalytic H_2 production for 30UiO-66/CIS nanocomposites. Reprinted with permission [125]. Copyright 2020, Elsevier

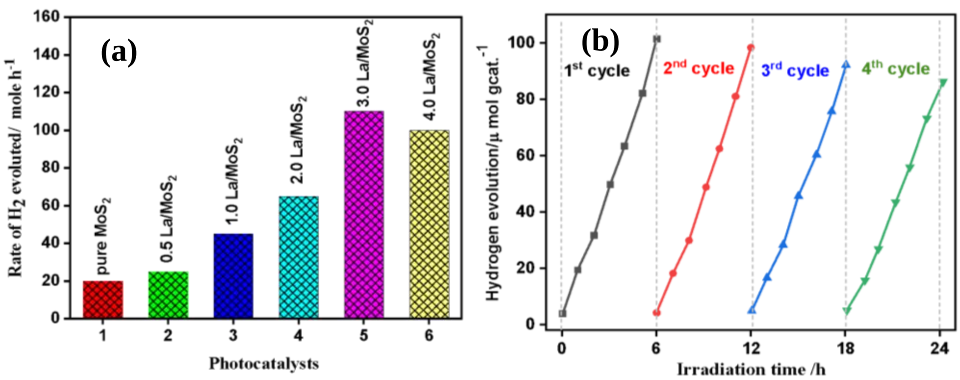

Figure 16. (a) Photocatalytic activity of different photocatalysts for H_2 production by the visible light source, and (b) the time course of photocatalytic H_2 production of 3%$LaMoS_2$ under visible light irradiation. Reprinted with permission[129]. Copyright 2015, Royal Society of Chemistry

5.2 Carbon dioxide reduction for fuel conversion

The conversion of CO_2 into fuels and high-value chemicals has garnered increasing global attention as it plays a significant role in reducing greenhouse gas emissions and generating valuable compounds. Consequently, CO_2 conversion and utilization should be regarded as essential elements for greenhouse gas reduction and sustainable long-term development.

Carbon dioxide (CO_2) is a fully oxidized molecule characterized by its thermodynamic stability and chemical inertness, making its activation particularly challenging. Additionally, when hydrocarbons are synthesized through the hydrogenation of CO_2, the process tends to yield short-chain hydrocarbons instead of the more desirable long-chain variants.

Consequently, much of the research in this area has focused on the selective hydrogenation of CO_2 into methane (CH_4), oxygenates, methanol (CH_3OH), formic acid (HCOOH), and light olefins, specifically those with carbon chain lengths ranging from two to four carbon atoms (C2–C4 olefins), as shown in **Figure 17** [134-140].

For example, Guodong Shi et al. efficiently synthesized flower-like MoS_2 utilizing a simple microwave hydrothermal process [141]. The vast amount of CO_2 adsorption can indefinitely furnish the initial reactant [142]. **Figure 18a** illustrates the CO_2 uptake behavior of as-synthesized samples at room temperature. Because it has the largest specific surface area, the nanocomposite Cu/MoS_2-1, and Cu/MoS_2-2 had a superior Carbon dioxide adsorption achievement than the pure MoS_2 and Cu/MoS_2-3. The maximum Carbon dioxide adsorption capacities of (Cu/MoS_2-1, Cu/MoS_2-2, Cu/MoS_2-3), and bare MoS_2 were 0.44, 0.41, 0.27, and 0.22 cm^{-3} g^{-1}, respectively. Cu/MoS_2-2 has a good CO_2 adsorption capacity after being interleaved with Cu nanoparticles. It is plausible to speculate that the significantly enhanced CO_2 adsorption contributed substantially to the better CO_2 reduction performance. Cu/MoS_2-2 exhibited a Tafel slope close to 126 mV dec^{-1}, but bare MoS_2 had one close to 264 mV dec^{-1}, as seen in **Figure 18b**. According to earlier studies [143], the differing Tafel slopes for both samples suggest that Cu/MoS_2 -2 had a significantly quicker electron transfer than bare flower-like MoS_2, endowing Cu/MoS_2 -2 with faster CO_2 reduction reaction kinetics. The increased electrical conductivity and better catalytic performance of Cu/MoS_2 -2 can be ascribed to a significant improvement in CO_2 electrochemical reduction performance. **Figure 18c** depicts a schematic depiction of CO_2 electro-chemical reduction over a Cu/MoS_2 sample.

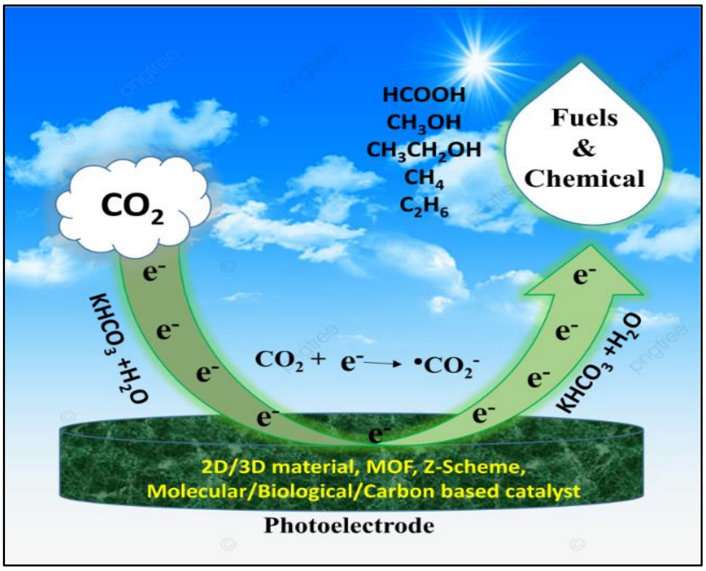

Figure 17. The illumination from solar light presents a diagram illustrating the photoelectrochemical (PEC) conversion of carbon dioxide into fuels and value-added products.

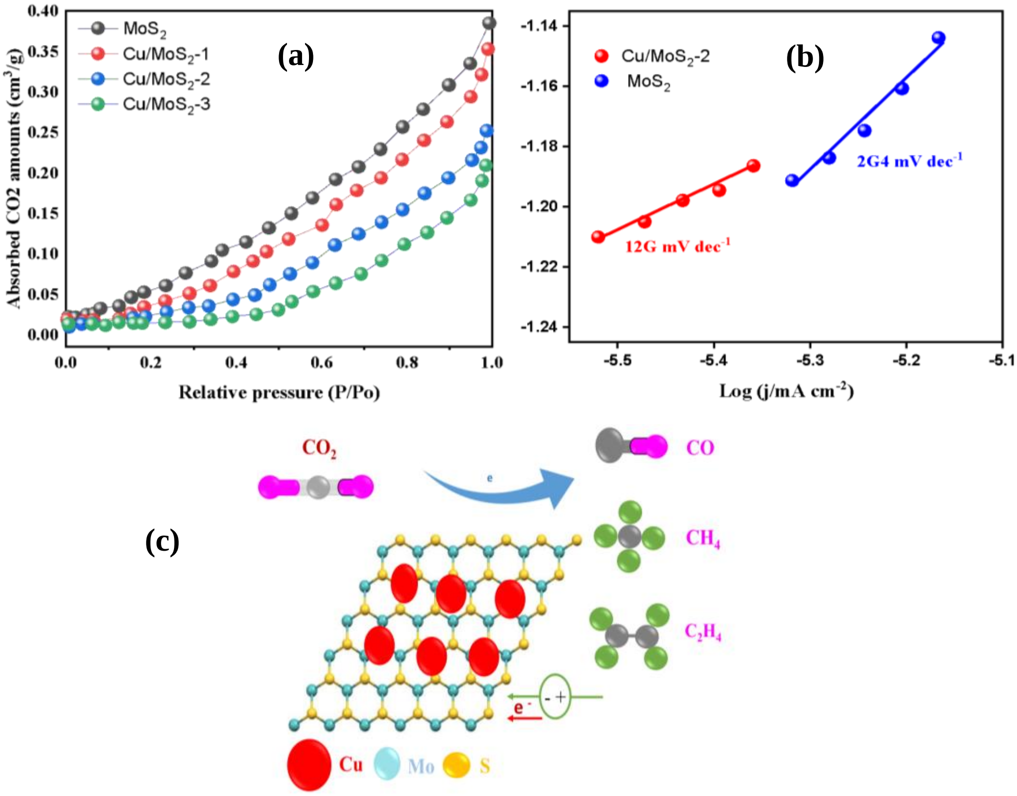

Figure 18. (a) The CO_2 adsorption isotherms, (b) Tafel plots for bare MoS_2 and Cu/MoS_2-2. (c) Diagram of the suggested CO_2 electro-reduction on the Cu/MoS_2 sample. Reprinted with permission [141]. © 2017, Royal Society of Chemistry

5.3 Removal of heavy metals from the water

Wastewater often contains various heavy metals, such as Zn, Pb, Cr, Cu, and Ni, etc., which are hazardous to aquatic life and the environment. Extracting metals from water is critical for environmental protection. There are several ways to remove metals from water [144-146], but adsorption is the most efficient. The most common application for activated carbon is as an adsorbent, although it has issues with desorption and regeneration. Titanates [147, 148] and silicates [149] were employed to solve this problem since they have unique surface characteristics. Titanate nanoflowers have been synthesized using thin nano-sheets and concentrated sodium hydroxide solution.

Multiple metal ions' adsorption behavior on (TNF) was investigated. The adsorption isotherms of total metal ions are shown in **Figure** 19a, b. TNF, TNT, and TNW have saturation capacities of 1.50, 0.68, and 0.42 mmol/g for the removal of multi-component ions (M (II) (**Figure** 19a). TNF's highest adsorption capacity for Cd (II), Ni (II), and Zn (II) ions was determined to be 0.73 mmol/g, 0.33 mmol/g, and 0.44 mmol/g, respectively. The impact of Zn (II) on Cd adsorption is seen in **Figure** 19c. Adding Zn (II) ions has a lesser influence on Cd (II) adsorption on TNF than on TNT and TNW. TNF's most excellent cadmium removal effectiveness is thus crucial for environmental protection and purifying cost savings [150].

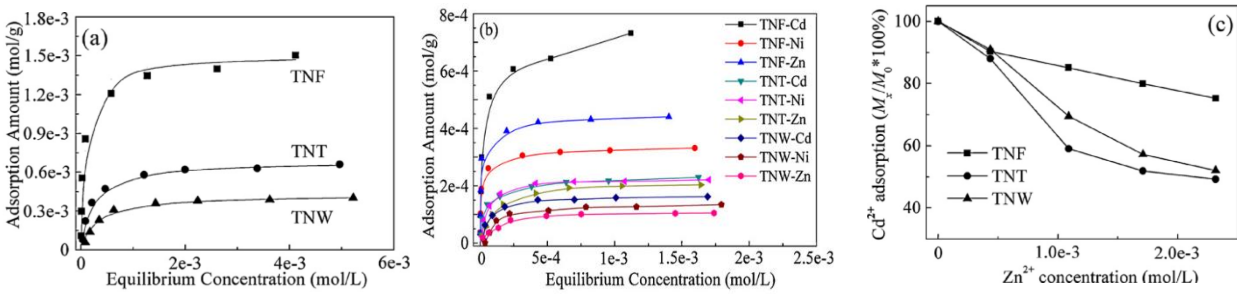

Figure 19 (a) The total metal ion adsorption isotherms, (b) Adsorption of ions from a mixed solution, and (c) Effect of Zn (II) on Cd (II) adsorption by different titanates (TNF, TNT, and TNW). Reprinted with permission [150]. Copyright 2012, Elsevier

5.4 Removal and degradation of organic dyes

Firstly, Several technologies, such as ion exchange, are employed for removing dyes from wastewater [151, 152], chemical oxidation [153], and adsorption [154], have been utilized. Nevertheless, the adsorption method stands out as a promising alternative treatment because of its straightforward operation, impressive efficiency, and minimal energy demand [155]. A variety of adsorbents, including activated carbon [156, 157], have successfully removed dyes from water.

Pankaj Singh Chauhan et al. described a new technique for producing consistently grown zinc oxide (ZnO) nanoflowers/(GO) composites on a silicon (Si) substrate [158]. In addition, the ZnO/GO photocatalyst was used to treat industrial wastewater from the ‘Common effluent treatment plant' (CETP) in Jodhpur, India, which included a combination of various dyes. This dye is made out of various industrial wastes from the textile and steel sectors. The UV-vis absorption spectrum of an industrial pigment after different irradiation periods with a ZnO/GO photocatalyst is shown in **Figure 20.** The dye was decolorized entirely in less than 100 minutes, quicker than prior work with metal coatings on ZnO nanorods [159].

A novel nanocomposite composed of chitosan (CS) and carbon nanoflowers (CNFs) was synthesized through the spray pyrolysis method for the purpose of dye removal from aqueous environments. The adsorption capabilities of this composite were evaluated in a batch mode assessment focusing on the elimination of two azo dyes: Acid Black 1 (AB1) and Congo Red (CR). Comprehensive investigations were conducted to determine the efficacy of the CS/CNFs composite in extracting these dyes from water. The study revealed that the maximum adsorption capacities of the CS/CNFs for AB1 and CR reached 259.13 mg g-1 and 553.12 mg g-1, respectively [160].

Secondly, the need for dye degradation has risen due to toxicity and carcinogenicity. This is because these colors are made up of highly toxic compounds (**Figure 21**). Dissolved oxygen in water is being depleted, and colors are being converted into carcinogenic or poisonous chemicals that can cause brain abnormalities and intestinal cancer [161]; microorganism growth inhibition, allergic responses, and certain dyes can even trigger a genetic mutation that leads to the creation of malignant tumors. [162, 163]. Because the dyes in the wastewater are aromatic chemicals like benzidine, they may be poisonous or carcinogenic. Hazardous waste removal is becoming more critical since its existence would cause numerous incurable ailments in living organisms [161].

Due to their distinctive physical and chemical properties not present in bulk materials, nanoflowers have been utilized in the reduction and elimination of harmful and toxic dyes, as shown in **Figure 22**.

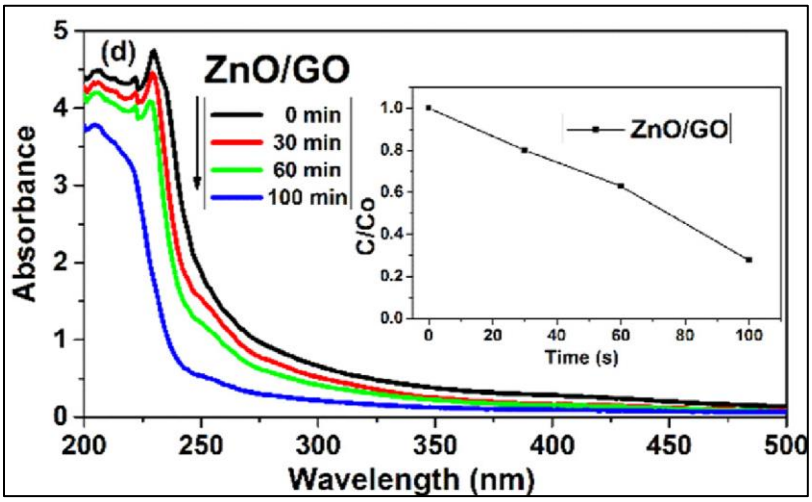

Figure 20. UV-vis absorption spectrum of an industrial dye using a ZnO/GO photocatalyst [158].

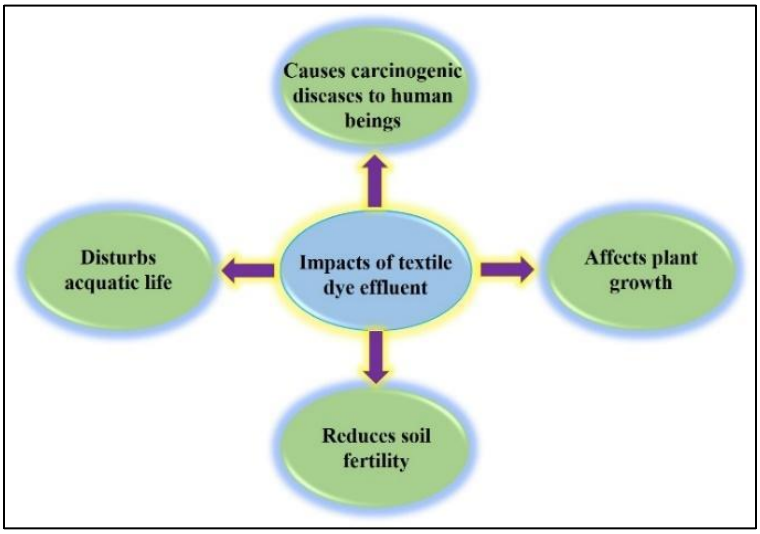

Figure 21: Impacts of textile dye effluent

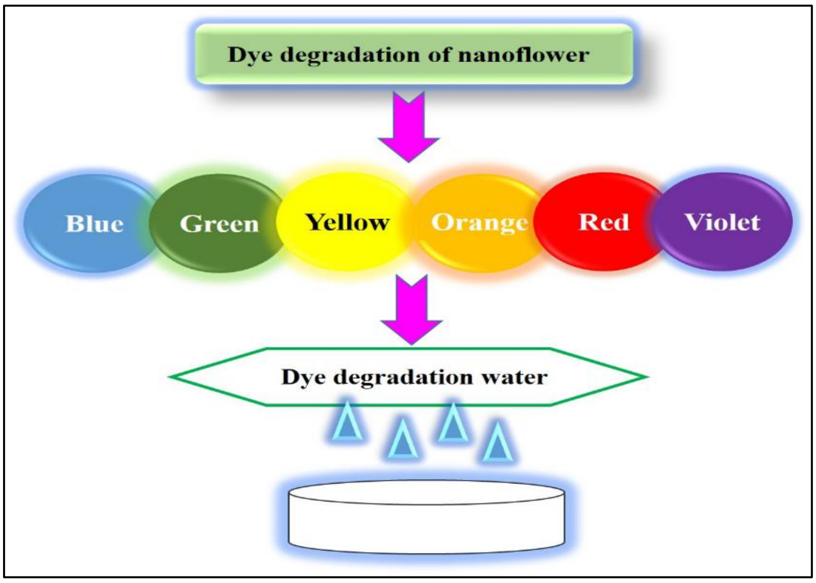

Figure 22: Dye degradation of nanoflowers.

For example, recently, our group developed flower-like AgI NP/BiOI NS composites. When BiOI nanoparticles and AgI nanosheets connect, they create a p-n heterostructure with nearly identical Fermi levels but different crystal structures on each side. Electrons in the conduction band edge of AgI nanoparticles easily move across the junction into the conduction band edge of BiOI. This separation of photogenerated electrons and holes greatly enhances photocatalytic efficiency. Upon exposure to light, the catalyst becomes excited and generates electron-hole pairs. These pairs react with environmental oxygen to form superoxide radicals. Additionally, the positive holes (h+) in the enhanced AgI/BiOI composites interact with adsorbed hydroxyl ions (OH-), resulting in the formation of hydroxyl radicals (●OH) when water oxidizes them. As demonstrated in **Figure 23**, these free radicals react with organic dye molecules to produce CO_2 and water (H_2O).

Additionally, the anthraquinone dye known as Reactive Blue 4 (RB4) served as a model dye for decolorization experiments using both free and immobilized laccase. (**Figure** 24a) [164]. The study explored how effectively both free laccase and laccase-lysine hybrid nanoflowers could decolorize substances, examining their performance with and without the presence of H_2O_2. which showed 59.81% (**Figure** 24b) and 73.60% (**Figure** 24d) decolorization after 1 hour of reaction, respectively. The RB4 underwent treatment with H2O2 to utilize the peroxidase-like activity exhibited by hybrid nanoflowers. Consequently, the decolorization efficiency of hybrid nanoflowers was enhanced to 89.46% (**Figure 24e**), despite free laccase's decolorization efficacy being unchanged (**Figure 24c**). According to these findings, the Combined activity of laccase-lysine hybrid nanoflowers decolorized Reactive blue four dye [165].

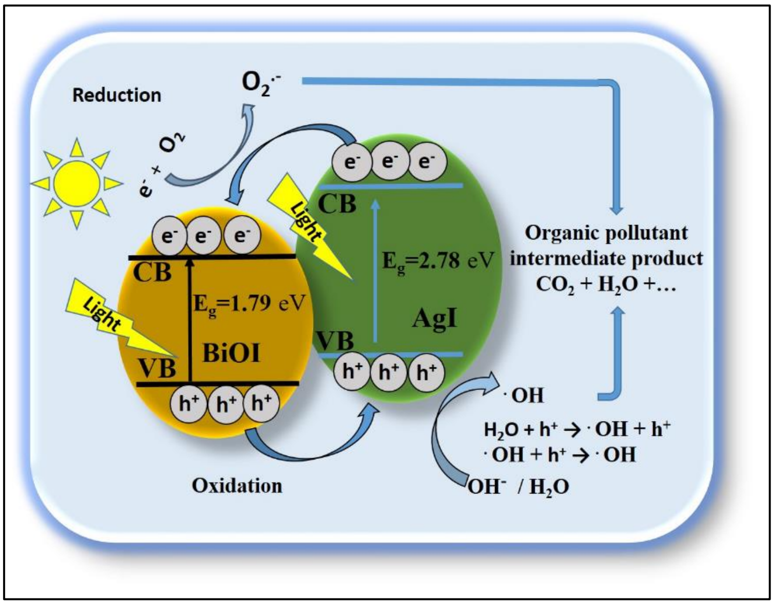

Figure 23. Diagram illustration as-photocatalytic of AgI NP/BiOI NS composite.

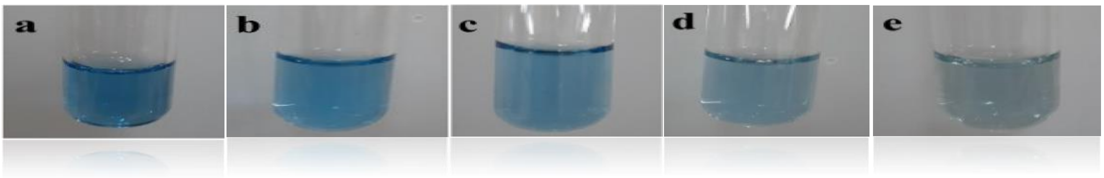

Figure 24. Photographs of organic dye for (a) The reactive blue dye (50 ppm) decolorization utilizing (b) free laccase, (c) The free laccase with H_2O_2, (d) The hybrid nano-flower, and (e) hybrid nano-flower with H_2O_2 after 1 hr. Reprinted with permission [164]. Copyright 2009, Taylor & Francis.

5.5 Nanoflower as supercapacitors in energy storage

Supercapacitors (SCs) are attracting much attention as a potential electrochemical energy storage technology [43, 124, 166-168]. SCs may be partly divided into two groups upen to the storage energy method. Electrochemical double-layer capacitors (EDLC) are a type of capacitor that uses the mechanism of electrostatic adsorption involves the attraction and accumulation of electrolyte ions on the surface of electrically conductive porous electrodes. This process is integral to the development of capacitance, as it enhances the ability of the electrodes to store and release electrical charge effectively. Pseudo-capacitors are another storage energy device that uses reversible redox processes at the electrode/electrolyte interface. Both methods are very dependent on the composition of the electrode materials, e.g., the kind of surface functions that determine the availability of pores, the conductivity of the materials, and the wettability of the electrodes. Nano-flower materials are the most frequently utilized electrodes in SCs due to their many well-known outstanding physicochemical features, including inexpensive manufacturing costs, high electrical conductivity, adjustable porosity, simplicity of processing, and the diversity of shapes they may take [169-171].

For instance, P. Rosaiah and co-workers synthesized RGO/Fe_3O_4 nanocomposites via an easy and cost-effective graphene thermal process to form the RGO/Fe_3O_4 nanocomposite, as shown in **Figure 25a**. This material features a substantial specific surface area of 141.3 m^2/g and an average pore size of 5.8 nm. The RGO/Fe3O4 nanocomposites used in supercapacitors displayed remarkable electrochemical performance. They achieved an impressive specific capacitance of 498 F/g at a scan rate of 10 mV/s and maintained 98.7% of their capacitance after 5,000 cycles at 500 mV/s when used as a supercapacitor electrode. Additionally, they retained 94% capacitance over more than 10,000 cycles at a current density of 3 A/g^{-1}. [172]. **(Figure 25b)**

M. Rajesh et al. synthesized Fe_3O_4 with rGO nanosheets to make up the flower-like Fe_3O_4/rGO hybrid nanocomposites. Fe_3O_4/rGO nanocomposites outperformed bare Fe_3O_4 nanoflowers and rGO sheets regarding specific capacitance (425 F/g at 1.5 A/g current density). Furthermore, even after 750 cycles at 3 A/g, 100% capacitance retention was found, as shown in **Figure 25c**. The results showed that enhanced electrode surface area, diffusion-controlled electron transfer kinetics, and a very stable Fe_3O_4/rGO matrix with a unique flower-like structure contributed to an exceptional electrochemical performance [173].

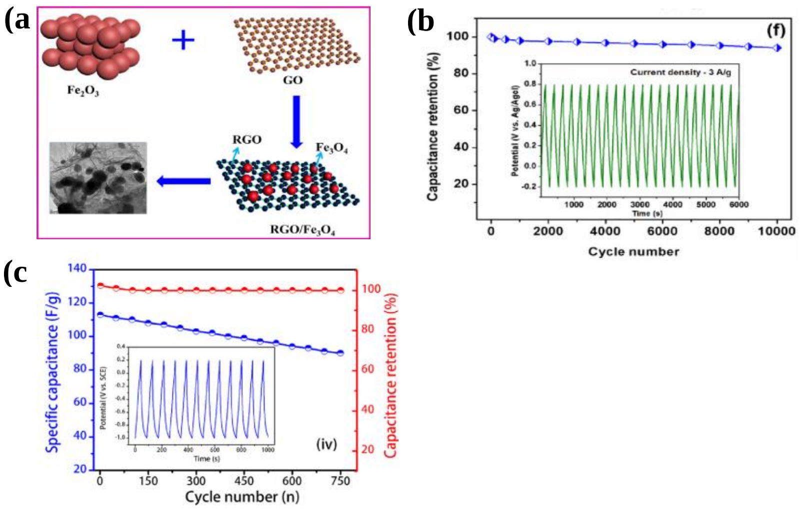

Figure 25 (a) The schematic of the preparation of RGO/Fe_3O_4 nanocomposite, (b) Capacitance retention at 3 A g^{-1} of RGO/Fe_3O_4 nanocomposite. Reprinted with permission [172]. Copyright 2019, Springer and (c) Cycling and capacitance retention efficiencies of Fe3O4/rGO composite. Reprinted with permission [173]. Copyright 2017, Elsevier

Zhihong Ai et al. prepared new 3D flower-like $CoNi_2S_4$/CNT composites fabricated via a precursor transformation process. The electrochemical performance of the materials was examined through cyclic voltammetry, galvanostatic charge-discharge tests, impedance spectroscopy, and cycle life assessments, as illustrated in Figure 26a-d. The CoNi2S4/carbon nanotube composites developed in this study demonstrated an exceptionally high specific capacitance of 2094 F g-1 at a current density of 1 A g-1, along with excellent rate capability, retaining 72% of their capacity at a higher current density of 10 A g^{-1}. [174, 175].

Recently, Chandu V. V. M. Gopi et al. prepared flower-like ZnO@$MnCo_2O_4$ nanosheets, and dandelion-like $MnCo_2O_4$ produced on nickel foam by hydrothermal technique with a brief post-annealing treatment. At a current density of 1 A g^{-1}, the flower-like ZnO@$MnCo_2O_4$ composite had a high capacitive performance of 631.2 F g^{-1} and high-density energy of 56.10 W h kg^{-1}, more significant than the dandelion-like $MnCo_2O_4$ electrode (452.5 F g^{-1}), as shown in **(Figure 27a-d)**. Over 1000 charge/discharge cycles, the flower-like ZnO@$MnCo_2O_4$ also displays outstanding cycling performance, showing good long-term cycling stability [176].

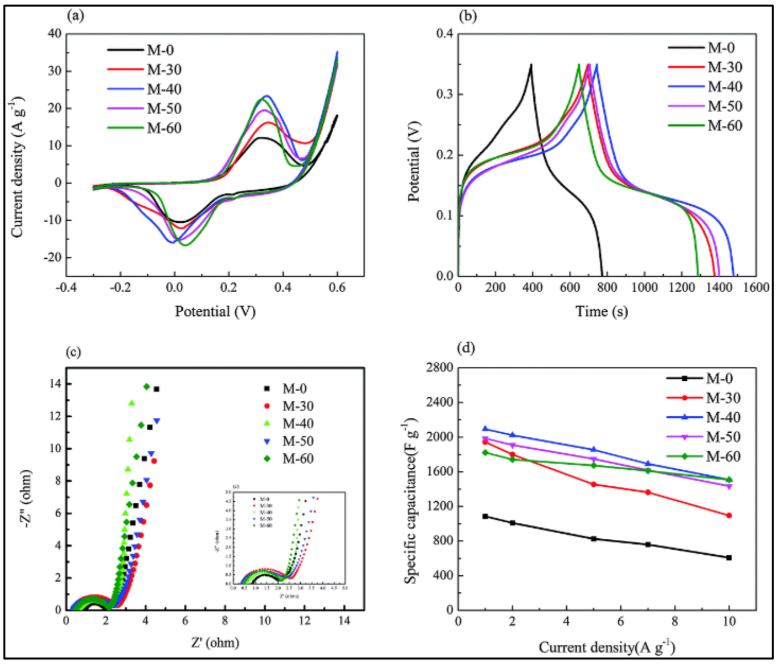

Figure 26 (a) Cyclic voltammetry; (b) the curves of charge and discharge; (c) Spectrums of impedance; (d) particular change with a current density for different samples. Reprinted with permission [174]. Copyright 2016, Royal Society of Chemistry

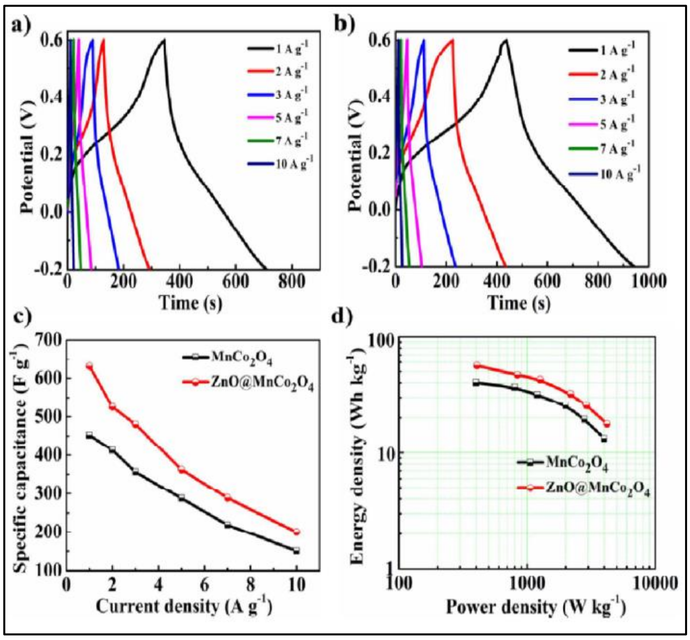

Figure 27. The curves of charge/ discharge of the (a) $MnCo_2O_4$ and (b) ZnO@$MnCo_2O_4$ electrodes; (c) the calculated-specific capacitance as a work of density, and (d) Ragone plot for the as-synthesis of $MnCo_2O_4$ and ZnO@$MnCo_2O_4$ electrodes. Reprinted with permission [176]. Copyright 2016, Royal Society of Chemistry

5.6 Application in lithium-ion batteries

Lithium batteries have gained popularity in electronic devices due to their lightweight design, high energy density, and comparatively long lifespan. While lithium is highly reactive and can ignite upon contact with water, modern lithium cells are chemically stabilized to prevent rapid reactions. Lithium cells come in various shapes and sizes, similar to nickel cells, but the lithium-ion cell is the most common nowadays [177].

Lithium-ion (Li-ion) batteries are widely used in a variety of portable devices, including smartphones, laptops, and digital cameras. This popularity stems from their lightweight nature, high energy storage capacity, and low self-discharge rate. [178, 179]. Commercial Li-ion batteries typically use transition metal oxide cathodes and graphitic carbon anodes, with one Li-ion intercalated every six C atoms, resulting in a theoretical capacity of 372 mA h g^{-1} [180]. Li-ions are deintercalated from the cathode and travel to the anode, where they intercalate in the graphite, allowing chemical energy to be converted to electrical energy. The discharging process is the inverse of that of charging [181].

For example, Xiaojia. Li et al. developed a hydrothermal approach using Flower-like nickel oxide/reduced graphene oxide nanocomposites (NiO/RGO) for lithium-ion battery applications [182]. After 100 cycles at a current density of 100 mA g^{-1}, the NiO/RGO nanocomposites show a better reversible lithium storage capacity of 702.3 mAh g^{-1}, accounting for retention of 77.0 % in comparison to the 2nd cycle, which is greater than that of pure NiO, as shown in **Figure 28a**.

Wenqiang Cao and his co-authors synthesized hierarchical 3D Co3O4 flowers with a monocrystal nanostructure using a facile two-step hydrothermal method. As shown in **Figure 28b**, the findings of 3D Co_3O_4 flower-like structures have a high reversible capacity of 920 mA h g^{-1} after 800 cycles at 1.12 C (1 C = 890 mA h g^{-1}), enhanced rate performance, and cycling stability. This study's findings open new possibilities for developing improved, long-lasting lithium-ion batteries [183].

Also, a straightforward two-step synthesis of densely interconnected cobalt molybdenum oxide ($CoMoO_4$) nanoparticles using MoS_2 nanoflowers as a sacrificial template Anode for lithium-ion batteries, is studied using an interconnected ($CoMoO_4$) nanoarchitecture generated from molybdenum sulfide [184]. At a current rate of C/5, the results of $CoMoO_4$ showed an outstanding discharge capacity of 1100 mA h g^{-1} over 100 cycles, as displayed in **Figure 28c**. Furthermore, after 500 cycles, the material showed improved electrochemical stability, high rate performance, and high discharge capacities of 600 and 220 mA h g^{-1}, respectively, at 5 C and 10 C.

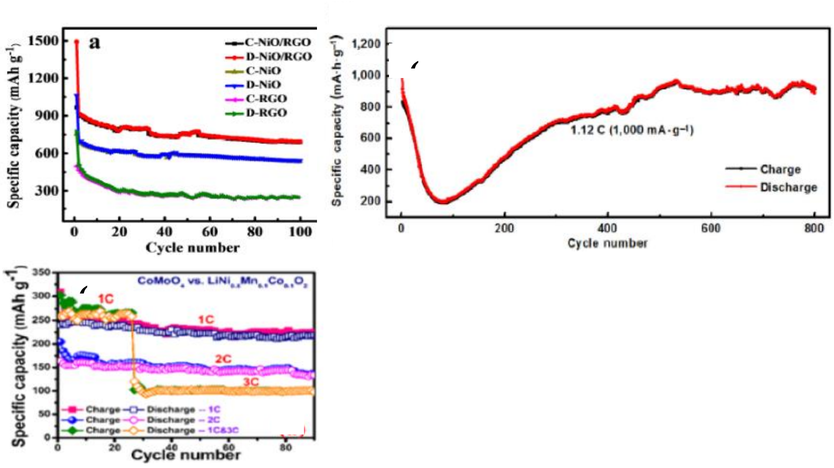

Figure 28. (a) The comparison of cycling performance of RGO, NiO, and NiO/RGO at 100 mA g-1. Reprinted with permission [182]. Copyright 2018, Elsevier, (b) Long cycling performance at a rate of 1.12 C. Reprinted with permission [183]. Copyright 2018, Springer, and (c) Capacity retention plots of CoMoO4. Reprinted with permission [184]. Copyright 2020, American Chemical Society.

Current and future developments

The fabrication of nanoflower-based structured materials with various well-established protocols has seen tremendous advances in previous decades. This review focuses on the current advances in nano-flower material production, characteristics, novel characterization techniques, and theoretical research. The use of nano-flower materials in specific, typical applications has also been discussed. Nanoflowers containing metal ions are classified based on their size and structure. The process of making nanoflowers is both cost-effective and environmentally benign. Nanoflowers hold significant potential in the pharmaceutical sector for applications such as protein drug delivery, anti-cancer treatments, multidrug delivery systems, toxicity and impurity testing, as well as in wastewater treatment. Research shows that nanoflowers' features rely on size and production procedures. Although the synthesis of nanoflower materials has received much interest in recent years, future research should focus on gaining a more profound knowledge of how synthetic methods, content, size, and shape impact material characteristics. Much work needs to be done in the area of low-cost manufacturing methodologies with the desirable morphologies and properties to discover new nanostructures of the requisite size and improve the manufacturing process management accuracy and speed.

There are intriguing new potentials and difficulties for materials scientists as progress is made in producing nanostructured nano-flower materials. Moreover, the actual reaction mechanisms of improved nano-flowers materials in performing applications in drug delivery, wastewater treatment, air purification, hydrogen production, and energy storage by the synthesis of nano-flowers followed by their reaction pathways have just become clear.

In addition, it is notable that the apparent quantum efficiency is lower even on large-scale and significant practical applications. Thus, in-depth research interest in nano-flower materials for sustainable chemistry can be expected, and more systematic work is indispensable. The structural methods, content, size, and shape are expected to be thoroughly investigated by coupling experimental results and computational simulations, further to improve the nano-flowers materials tool in any upcoming research. We anticipate that the current review article will encourage further development of nanoflower-based structured materials and their application to address the current and future environmental and energy-related demands.

Acknowledgment

This publication's research was supported by several sponsors: the National Natural Science Foundation of China (Project No. 21572180), the Intergovernmental Science and Technology Directorate Cooperation and Exchange Program between China and Romania (Project No. 43-24 20180510), the Natural Science Basic Research Plan in Shaanxi Province of China (Project No. 2012JZ2002), and the Academic Funding of Northwestern Polytechnical University (NPU, Project Nos. 17GH0402 and W212002). We extend our sincere gratitude to the Analytical and Testing Center of Northwestern Polytechnical University for granting access to the essential laboratory facilities.

Conflict of interest: NIL

References

[1] F.L. Gaol, J. Webb, Recent Trends in Nanotechnology and Materials Science: Selected Review Papers from the 2013 International Conference on Manufacturing, Optimization, Industrial and Material Engineering (MOIME 2013), Springer2014.

[2] A. Rahi, N. Sattarahmady, H. Heli, Label-free electrochemical aptasensing of the human prostate-specific antigen using gold nanospears, Talanta, 156 (2016) 218-224.

[3] N. Sattarahmady, H. Heli, A. Moosavi-Movahedi, An electrochemical acetylcholine

biosensor based on nanoshells of hollow nickel microspheres-carbon microparticles-Nafion nanocomposite, Biosensors and Bioelectronics, 25 (2010) 2329-2335.

[4] H. Heli, S. Majdi, N. Sattarahmady, A. Parsaei, Electrocatalytic oxidation and sensitive detection of deferoxamine on nanoparticles of Fe 2 O 3@ NaCo [Fe (CN) 6]-modified paste electrode, Journal of Solid State Electrochemistry, 14 (2010) 1637-1647.

[5] H. Heli, S. Majdi, N. Sattarahmady, Fe2O3 core–NaCo [Fe (CN) 6] shell nanoparticles—Synthesis and characterization, Materials Research Bulletin, 45 (2010) 850-858.

[6] N. Sattarahmady, A. Parsa, H. Heli, Albumin nanoparticle-coated carbon composite electrode for electrical double-layer biosupercapacitor applications, Journal of Materials Science, 48 (2013) 2346-2351.

[7] Yameny, A. A Comprehensive Review on Nanoparticles: Definition, Preparation, Characterization, Types, and Medical Applications. *Journal of Medical and Life Science*, 2024; 6(4): 663-672. doi: 10.21608/jmals.2024.419629.

[8] H. Heli, H. Yadegari, Nanoflakes of the cobaltous oxide, CoO: Synthesis and characterization, Electrochimica Acta, 55 (2010) 2139-2148.

[9] N. Sattarahmady, H. Heli, F. Faramarzi, Nickel oxide nanotubes-carbon microparticles/Nafion nanocomposite for the electrooxidation and sensitive detection of metformin, Talanta, 82 (2010) 1126-1135.

[10] N. Sattarahmady, R.D. Vais, H. Heli, Fibroin nanofibrils as an electrode material for electrical double-layer biosupercapacitor applications, Journal of Applied Electrochemistry, 45 (2015) 577-583.

[11] H. Heli, H. Yadegari, A. Jabbari, Investigation of the lithium intercalation behavior of nanosheets of LiV3O8 in an aqueous solution, The Journal of Physical Chemistry C, 115 (2011) 10889-10897.

[12] Q. Abbas, S.H. Siyal, A. Mateen, M.A. Bajaber, A. Ahmad, M.S. Javed, P. Martin, N. Joly, P. Bocchetta, Flower-like highly open-structured binder-free Zn-Co-oxide nanosheet for high-performance supercapacitor electrodes, Molecules, 27 (2022) 4850.

[13] Y. Zhang, C. Li, C. Zhou, L. Lv, M. Ma, K. Yao, L. Yu, 3D flower-like architectures assembled by ZnO porous nanosheets with higher surface area for enhanced lower temperature NO 2 gas sensors, Journal of Materials Chemistry C, 13 (2025) 7686-7695.

[14] A. Rahi, N. Sattarahmady, R.D. Vais, H. Heli, Sonoelectrodeposition of gold nanorods at a gold surface–application for electrocatalytic reduction and determination of nitrofurazone, Sensors and Actuators B: Chemical, 210 (2015) 96-102.

[15] N. Bashir, S. Zulfiqar, S. Munir, M.M. Ibrahim, M.F. Abou Taleb, S.M. El-Bahy, M. Suleman, M. Shahid, Sodium doped-V2O5 nanorods for visible light irradiated photocatalytic performance for the degradation of Rh-dye, Ceramics International, 48 (2022) 10932-10940.

[16] H. Heli, J. Pishahang, H.B. Amiri, Synthesis of hexagonal CoAl-layered double hydroxide nanoshales/carbon nanotubes composite for the non-enzymatic detection of hydrogen peroxide, Journal of Electroanalytical Chemistry, 768 (2016) 134-144.

[17] J. Ge, J. Lei, R.N. Zare, Protein–inorganic hybrid nanoflowers, Nature nanotechnology, 7 (2012) 428-432.

[18] X. Hu, J. Hu, J. Tian, Z. Ge, G. Zhang, K. Luo, S. Liu, Polyprodrug amphiphiles: hierarchical assemblies for shape-regulated cellular internalization, trafficking, and drug delivery, Journal of the American Chemical Society, 135 (2013) 17617-17629.

[19] J.B. Lee, J. Hong, D.K. Bonner, Z. Poon, P.T. Hammond, Self-assembled RNA interference microsponges for efficient siRNA delivery, Nature Materials, 11 (2012) 316-322.

[20] D. Shcharbin, I. Halets-Bui, V. Abashkin, V. Dzmitruk, S. Loznikova, M. Odabaşı, Ö. Acet, B. Önal, N. Özdemir, N. Shcharbina, Hybrid metal-organic nanoflowers and their application in biotechnology and medicine, Colloids and Surfaces B: Biointerfaces, 182 (2019) 110354.

[21] T.D. Tran, M.I. Kim, Organic-inorganic hybrid nanoflowers as potent materials for biosensing and biocatalytic applications, BioChip Journal, 12 (2018) 268-279.

[22] J. Cui, S. Jia, Organic–inorganic hybrid nanoflowers: A novel host platform for immobilizing biomolecules, Coordination Chemistry Reviews, 352 (2017) 249-263.

[23] H. Heli, A. Rahi, Synthesis and applications of nanoflowers, Recent patents on nanotechnology, 10 (2016) 86-115.

[24] B.I. Kharisov, A review for synthesis of nanoflowers, Recent patents on nanotechnology, 2 (2008) 190-200.

[25] G. Zhang, C. Deng, H. Shi, B. Zou, Y. Li, T. Liu, W. Wang, ZnO/Ag composite nanoflowers as substrates for surface-enhanced Raman scattering, Applied Surface Science, 402 (2017) 154-160.

[26] R. Yang, H. Li, Y. Wang, Z. Zhu, C. Hu, T. Zhao, W. Wang, B. Liu, A novel flower-like Z-type heterojunction CuS/Bi 7 O 9 I 3 composite catalyst prepared under mild conditions for degradation of antibiotics and sterilization under visible light, Environmental Science: Nano, 7 (2020) 3074-3087.

[27] H. Wang, Q. Lin, L. Yin, Y. Yang, Y. Qiu, C. Lu, H. Yang, Biomimetic Design of Hollow Flower-Like g-C3N4@ PDA Organic Framework Nanospheres for Realizing an Efficient Photoreactivity, Small, 15 (2019) 1900011.

[28] H. Zhang, S. Tan, D. Wang, J. Wu, W. Xu, S. Zhao, X. Sun, Q. Liu, H. Liu, Y. Guan, Fabrication of bionic flower-like g-C3N4/Bi4O5I2 photocatalyst with enhanced photocatalytic performance, Chemical Physics Letters, 751 (2020) 137533.

[29] M. Siahmansouri, M. Mousavi-Kamazani, Photocatalytic desulfurization of thiophene under visible light by hollow flower-like NixZn2-xV2O7/WO4 nanostructures, Ceramics International, (2021).

[30] M. Mousavi-Kamazani, M. Ghodrati, R. Rahmatolahzadeh, Fabrication of Z-scheme flower-like AgI/Bi 2 O 3 heterojunctions with enhanced visible light photocatalytic desulfurization under mild conditions, Journal of Materials Science: Materials in Electronics, 31 (2020) 5622-5634.

[31] O. Amiri, F. Beshkar, S.S. Ahmed, A. Rafiei-Miandashti, P.H. Mahmood, A.A. Dezaye, Novel flower-like (Bi (Bi2S3) 9I3) 2/3 nanostructure as efficient photocatalyst for photocatalytic desulfurization of benzothiophene under visible light irradiation, Advanced Powder Technology, 32 (2021) 1088-1098.

[32] L. Qi, Y. Yang, P. Zhang, Y. Le, C. Wang, T. Wu, Hierarchical flower-like BiOIxBr (1− x) solid solution spheres with enhanced visible-light photocatalytic activity, Applied Surface Science, 467 (2019) 792-801.

[33] Z. Yang, R. Wang, L. Xu, C. Liu, Y. Cheng, Z. Jiang, Y. Liu, T. Zhang, J. Li, X. Liu, Highly efficient flower-like Dy3+-doped Bi2MoO6 photocatalyst under simulated sunlight: Design, fabrication and characterization, Optical Materials, 116 (2021) 111094.

[34] J. Wu, Y. Xie, Y. Ling, Y. Dong, J. Li, S. Li, J. Zhao, Synthesis of flower-like g-C3N4/BiOBr and enhancement of the activity for the degradation of bisphenol A under

visible light irradiation, Frontiers in Chemistry, 7 (2019) 649.

[35] W. Peng, W. Wang, G. Han, Y. Huang, Y. Zhang, Fabrication of 3D flower-like MoS2/graphene composite as high-performance electrode for capacitive deionization, Desalination, 473 (2020) 114191.

[36] J. Shi, S. Zhang, X. Wang, C. Yang, Z. Jiang, Preparation and enzymatic application of flower-like hybrid microcapsules through a biomimetic mineralization approach, Journal of Materials Chemistry B, 2 (2014) 4289-4296.

[37] Y. Song, J. Gao, Y. He, L. Zhou, L. Ma, Z. Huang, Y. Jiang, Preparation of a flowerlike nanobiocatalyst system via biomimetic mineralization of cobalt phosphate with enzyme, Industrial & Engineering Chemistry Research, 56 (2017) 14923-14930.

[38] Y. Liu, J. Chen, M. Du, X. Wang, X. Ji, Z. He, The preparation of dual-functional hybrid nanoflower and its application in the ultrasensitive detection of disease-related biomarker, Biosensors and Bioelectronics, 92 (2017) 68-73.

[39] Y. Liu, X. Xu, J. Zhang, H. Zhang, W. Tian, X. Li, M.O. Tade, H. Sun, S. Wang, Flower-like MoS2 on graphitic carbon nitride for enhanced photocatalytic and electrochemical hydrogen evolutions, Applied Catalysis B: Environmental, 239 (2018) 334-344.

[40] Y. Tang, Y. Liu, S. Yu, Y. Zhao, S. Mu, F. Gao, Hydrothermal synthesis of a flower-like nano-nickel hydroxide for high performance supercapacitors, Electrochimica Acta, 123 (2014) 158-166.

[41] S. Liu, H. Li, L. Yan, Z. Wang, H. Liu, Synthesis, characterisation and adsorption/photocatalytic performance of ZnO/CdS flowers, Micro & Nano Letters, 8 (2013) 827-831.

[42] M. Li, H. Yu, R. Huang, F. Bai, M. Trevor, D. Song, B. Jiang, Y. Li, Facile one-pot synthesis of flower-like AgCl microstructures and enhancing of visible light photocatalysis, Nanoscale research letters, 8 (2013) 1-6.

[43] J. Ma, S. Zhu, Q. Shan, S. Liu, Y. Zhang, F. Dong, H. Liu, Facile synthesis of flower-like (BiO) 2CO3@ MnO2 and Bi2O3@ MnO2 nanocomposites for supercapacitors, Electrochimica Acta, 168 (2015) 97-103.

[44] H. Zhou, S. Xiong, L. Wei, B. Xi, Y. Zhu, Y. Qian, Acetylacetone-Directed Controllable Synthesis of Bi2S3 Nanostructures with Tunable Morphology, Crystal Growth & Design, 9 (2009) 3862-3867.

[45] L. Wang, T. Zhang, J. Su, L. Guo, Room-temperature photodeposition of conformal transition metal based cocatalysts on BiVO 4 for enhanced photoelectrochemical water splitting, Nano Research, 13 (2020) 231-237.

[46] J. Hasan, G. Ouyang, J. Wang, H. Li, G. Tian, C. Qin, Efficient Visible-light-driven Photocatalysis of Flower-like Composites of AgI nanoparticle/BiOI nanosheet, Journal of Solid State Chemistry, (2021) 122044.

[47] H. Saricimen, A. Ul-Hamid, A. Quddus, Effect of calcination on nanoscale zirconia produced by high temperature hydrolysis, Protection of Metals and Physical Chemistry of Surfaces, 51 (2015) 803-811.

[48] A. Al-Fatesh, A. Fakeeha, Effects of calcination and activation temperature on dry reforming catalysts, Journal of Saudi Chemical Society, 16 (2012) 55-61.

[49] J. Chen, L. Zhu, Y. Xiang, D. Xia, Effect of calcination temperature on structural properties and catalytic performance of novel amorphous NiP/Hβ catalyst for n-Hexane isomerization, Catalysts, 10 (2020) 811.

[50] H. Lv, X. Liang, G. Ji, H. Zhang, Y. Du, Porous three-dimensional flower-like Co/CoO and its excellent electromagnetic

absorption properties, ACS applied materials & interfaces, 7 (2015) 9776-9783.

[51] Y.X. Gan, A.H. Jayatissa, Z. Yu, X. Chen, M. Li, Hydrothermal synthesis of nanomaterials, Hindawi, 2020.

[52] F. Shi, F. Wang, H. Dai, J. Dai, J. Deng, Y. Liu, G. Bai, K. Ji, C.T. Au, Rod-, flower-, and dumbbell-like MnO2: Highly active catalysts for the combustion of toluene, Applied Catalysis A: General, 433 (2012) 206-213.

[53] X. Liu, Z. Xing, Y. Zhang, Z. Li, X. Wu, S. Tan, X. Yu, Q. Zhu, W. Zhou, Fabrication of 3D flower-like black N-TiO2-x@ MoS2 for unprecedented-high visible-light-driven photocatalytic performance, Applied Catalysis B: Environmental, 201 (2017) 119-127.

[54] S. Mashhadi, H. Javadian, M. Ghasemi, T.A. Saleh, V.K. Gupta, Microwave-induced H2SO4 activation of activated carbon derived from rice agricultural wastes for sorption of methylene blue from aqueous solution, Desalination and Water Treatment, 57 (2016) 21091-21104.

[55] V. Polshettiwar, M.N. Nadagouda, R.S. Varma, Microwave-assisted chemistry: a rapid and sustainable route to synthesis of organics and nanomaterials, Australian Journal of Chemistry, 62 (2009) 16-26.

[56] J.S. Souza, F.T. Hirata, P. Corio, Microwave-assisted synthesis of bismuth vanadate nanoflowers decorated with gold nanoparticles with enhanced photocatalytic activity, Journal of Nanoparticle Research, 21 (2019) 35.

[57] T.A. Saleh, S. Majeed, A. Nayak, B. Bhushan, Principles and advantages of microwave-assisted methods for the synthesis of nanomaterials for water purification, Advanced nanomaterials for water engineering, treatment, and hydraulics, IGI Global2017, pp. 40-57.

[58] D. Nath, P. Banerjee, Green nanotechnology–a new hope for medical biology, Environmental Toxicology and Pharmacology, 36 (2013) 997-1014.

[59] M. Razavi, E. Salahinejad, M. Fahmy, M. Yazdimamaghani, D. Vashaee, L. Tayebi, Green chemical and biological synthesis of nanoparticles and their biomedical applications, Green processes for nanotechnology, (2015) 207-235.

[60] K.B. Narayanan, N. Sakthivel, Green synthesis of biogenic metal nanoparticles by terrestrial and aquatic phototrophic and heterotrophic eukaryotes and biocompatible agents, Advances in Colloid and Interface Science, 169 (2011) 59-79.

[61] J.-Y. Dong, C.-H. Lin, Y.-J. Hsu, S.-Y. Lu, D.S.-H. Wong, Single-crystalline mesoporous ZnO nanosheets prepared with a green antisolvent method exhibiting excellent photocatalytic efficiencies, CrystEngComm, 14 (2012) 4732-4737.

[62] J.K. Rajput, T.K. Pathak, H.C. Swart, L.P. Purohit, Synthesis of CdO nanoflowers by Sol-Gel method on different substrates with photodetection application, physica status solidi (a), 216 (2019) 1900093.

[63] S. Thiagarajan, A. Sanmugam, D. Vikraman, Facile methodology of sol-gel synthesis for metal oxide nanostructures, recent applications in sol-gel synthesis, (2017) 1-17.

[64] S.F. Mousavi, F. Davar, M. Loghman-Estarki, Controllable synthesis of ZnO nanoflowers by the modified sol–gel method, Journal of Materials Science: Materials in Electronics, 27 (2016) 12985-12995.

[65] A. Nagar, A. Kumar, S. Parveen, A. Kumar, H. Dhasmana, S. Husain, A. Verma, V. Jain, Zinc oxide nanoflowers synthesized by sol-gel technique for field emission displays (FEDs), Materials Today: Proceedings, 32 (2020) 402-406.

[66] K. Haouemi, F. Touati, N. Gharbi, Characterization of a new TiO 2 nanoflower prepared by the sol–gel process in a reverse microemulsion, Journal of Inorganic and Organometallic Polymers and Materials, 21 (2011) 929-936.

[67] F. Nasirpouri, K. Alipour, F. Daneshvar, M.-R. Sanaeian, Electrodeposition of anticorrosion nanocoatings, Corrosion Protection at the Nanoscale, Elsevier2020, pp. 473-497.

[68] Z. Cai, Q. Yao, X. Chen, X. Wang, Nanomaterials With Different Dimensions for Electrocatalysis, Novel Nanomaterials for Biomedical, Environmental and Energy Applications, Elsevier2019, pp. 435-464.

[69] P. Dhanasekaran, K. Lokesh, P. Ojha, A. Sahu, S. Bhat, D. Kalpana, Electrochemical deposition of three-dimensional platinum nanoflowers for high-performance polymer electrolyte fuel cells, Journal of Colloid and Interface Science, 572 (2020) 198-206.

[70] H. Zhang, W. Zhou, Y. Du, P. Yang, C. Wang, One-step electrodeposition of platinum nanoflowers and their high efficient catalytic activity for methanol electro-oxidation, Electrochemistry Communications, 12 (2010) 882-885.

[71] J. Zhou, Y. Zhao, J. Bao, D. Huo, H. Fa, X. Shen, C. Hou, One-step electrodeposition of Au-Pt bimetallic nanoparticles on MoS2 nanoflowers for hydrogen peroxide enzyme-free electrochemical sensor, Electrochimica Acta, 250 (2017) 152-158.

[72] L. Qian, X. Yang, Polyamidoamine dendrimers-assisted electrodeposition of gold− platinum bimetallic nanoflowers, The Journal of Physical Chemistry B, 110 (2006) 16672-16678.

[73] A.A. Firooz, A.R. Mahjoub, A.A. Khodadadi, Highly sensitive CO and ethanol nanoflower-like SnO2 sensor among various morphologies obtained by using single and mixed ionic surfactant templates, Sensors and Actuators B: Chemical, 141 (2009) 89-96.

[74] Y. Lai, M. Meng, Y. Yu, X. Wang, T. Ding, Photoluminescence and photocatalysis of the flower-like nano-ZnO photocatalysts prepared by a facile hydrothermal method with or without ultrasonic assistance, Applied Catalysis B: Environmental, 105 (2011) 335-345.

[75] Q. Gao, A. Zhao, Z. Gan, W. Tao, D. Li, M. Zhang, H. Guo, D. Wang, H. Sun, R. Mao, Facile fabrication and growth mechanism of 3D flower-like Fe 3 O 4 nanostructures and their application as SERS substrates, CrystEngComm, 14 (2012) 4834-4842.

[76] Z. Shen, Q. Zhang, C. Yin, S. Kang, H. Jia, X. Li, X. Li, Y. Wang, L. Cui, Facile synthesis of 3D flower-like mesoporous Ce-ZnO at room temperature for the sunlight-driven photocatalytic degradations of RhB and phenol, Journal of colloid and interface science, 556 (2019) 726-733.

[77] Z. Yang, W. Qi, R. Su, Z. He, 3D flower-like micro/nano Ce–Mo composite oxides as effective bifunctional catalysts for one-pot conversion of fructose to 2, 5-diformylfuran, ACS Sustainable Chemistry & Engineering, 5 (2017) 4179-4187.

[78] A. Chatterjee, P. Kar, D. Wulferding, P. Lemmens, S.K. Pal, Flower-like BiOI microspheres decorated with plasmonic gold nanoparticles for dual detoxification of organic and inorganic water pollutants, ACS Applied Nano Materials, 3 (2020) 2733-2744.

[79] L. Hao, P. Ju, Y. Zhang, X. Zhai, C. Sun, J. Duan, Y. Su, Z. Lu, D. Liao, Fabrication of hierarchical flower-like BiOI/MoS2 heterostructures with highly enhanced visible-light photocatalytic activities, Colloids and Surfaces A: Physicochemical and Engineering Aspects, 610 (2021) 125714.

[80] Y. Chen, Y. Liu, X. Xie, C. Li, Y. Si, M. Zhang, Q. Yan, Synthesis flower-like BiVO 4/BiOI core/shell heterostructure photocatalyst for tetracycline degradation under visible-light irradiation, Journal of Materials Science: Materials in Electronics, 30 (2019) 9311-9321.

[81] A.-J. Wang, S.-F. Qin, D.-L. Zhou, L.-Y. Cai, J.-R. Chen, J.-J. Feng, Caffeine assisted one-step synthesis of flower-like gold nanochains and their catalytic behaviors, RSC Advances, 3 (2013) 14766-14773.

[82] W. Feng, L. Chen, M. Qin, X. Zhou, Q. Zhang, Y. Miao, K. Qiu, Y. Zhang, C. He, Flower-like PEGylated MoS 2 nanoflakes for near-infrared photothermal cancer therapy, Scientific Reports, 5 (2015) 1-13.

[83] P. Qu, Z. Gong, H. Cheng, W. Xiong, X. Wu, P. Pei, R. Zhao, Y. Zeng, Z. Zhu, Nanoflower-like CoS-decorated 3D porous carbon skeleton derived from rose for a high performance nonenzymatic glucose sensor, RSC Advances, 5 (2015) 106661-106667.

[84] A.K. Barui, V. Veeriah, S. Mukherjee, J. Manna, A.K. Patel, S. Patra, K. Pal, S. Murali, R.K. Rana, S. Chatterjee, Zinc oxide nanoflowers make new blood vessels, Nanoscale, 4 (2012) 7861-7869.

[85] D. Meng, C. He, L. Zhang, Y. Zhang, R. Li, K. Tao, X. San, Design of 3D flower-like NiWO 4/WO 3 heterostructures with excellent trimethylamine sensing performance, CrystEngComm, 26 (2024) 3547-3556.

[86] Y. Garini, B.J. Vermolen, I.T. Young, From micro to nano: recent advances in high-resolution microscopy, Current opinion in biotechnology, 16 (2005) 3-12.

[87] D. Semwogerere, E.R. Weeks, Confocal microscopy, Encyclopedia of biomaterials and biomedical engineering, 23 (2005) 1-10.

[88] O. de Oliveira Jr, L. Ferreira, G. Marystela, F. de Lima Leite, A.L. Da Róz, Nanocharacterization techniques, William Andrew2017.

[89] S. Boddolla, S. Thodeti, A review on characterization techniques of nanomaterials, International Journal of Engineering, Science and Mathematics, 7 (2018) 169-175.

[90] M. Carter, J.C. Shieh, Guide to research techniques in neuroscience, Academic Press2015.

[91] A.M. Pinto, V.S. Oliveira, D.S.C. Falcao, Direct Alcohol Fuel Cells for Portable Applications: Fundamentals, Engineering and Advances, Academic Press2018.

[92] J. Liang, S. Chen, M. Xie, Y. Wang, X. Guo, X. Guo, W. Ding, Expeditious fabrication of flower-like hierarchical mesoporous carbon superstructures as supercapacitor electrode materials, Journal of Materials Chemistry A, 2 (2014) 16884-16891.

[93] B. Inkson, Scanning electron microscopy (SEM) and transmission electron microscopy (TEM) for materials characterization, Materials characterization using nondestructive evaluation (NDE) methods, Elsevier2016, pp. 17-43.

[94] K.E. Ramohlola, E.I. Iwuoha, M.J. Hato, K.D. Modibane, Instrumental Techniques for Characterization of Molybdenum Disulphide Nanostructures, Journal of Analytical Methods in Chemistry, 2020 (2020).

[95] M. Joshi, A. Bhattacharyya, S.W. Ali, Characterization techniques for nanotechnology applications in textiles, (2008).

[96] N. Jalili, K. Laxminarayana, A review of atomic force microscopy imaging systems: application to molecular metrology and biological sciences, Mechatronics, 14 (2004) 907-945.

[97] Q. Liu, H. Yang, Application of atomic force microscopy in food microorganisms, Trends in food science & technology, 87 (2019) 73-83.

[98] R.A. Ismail, A.-M.E. Al-Samarai, S.J. Mohmed, H.H. Ahmed, Characteristics of nanostructured CdO/Si heterojunction photodetector synthesized by CBD, Solid-state electronics, 82 (2013) 115-121.

[99] A.A. Bunaciu, E.G. UdriŞTioiu, H.Y. Aboul-Enein, X-ray diffraction: instrumentation and applications, Critical reviews in analytical chemistry, 45 (2015) 289-299.

[100] P. Singh, Y.J. Kim, C. Wang, R. Mathiyalagan, D.C. Yang, Microbial synthesis of flower-shaped gold nanoparticles, Artificial cells, nanomedicine, and biotechnology, 44 (2016) 1469-1474.

[101] Z.-F. Wu, Z. Wang, Y. Zhang, Y.-L. Ma, C.-Y. He, H. Li, L. Chen, Q.-S. Huo, L. Wang, Z.-Q. Li, Amino acids-incorporated nanoflowers with an intrinsic peroxidase-like activity, Scientific reports, 6 (2016) 1-7.

[102] K. Ren, K. Zhang, J. Liu, H. Luo, Y. Huang, X. Yu, Controllable synthesis of hollow/flower-like BiOI microspheres and highly efficient adsorption and photocatalytic activity, CrystEngComm, 14 (2012) 4384-4390.

[103] C.V. Reddy, R.R. Kakarla, B. Cheolho, J. Shim, M. Rezakazemi, T.M. Aminabhavi, Highly efficient photodegradation of toxic organic pollutants using Cu-doped V2O5 nanosheets under visible light, Chemosphere, 311 (2023) 137015.

[104] C.J. Chirayil, J. Abraham, R.K. Mishra, S.C. George, S. Thomas, Instrumental techniques for the characterization of nanoparticles, Thermal and Rheological Measurement Techniques for Nanomaterials Characterization, Elsevier2017, pp. 1-36.

[105] J. Hasan, H. Li, G. Tian, C. Qin, Fabrication of Cr2S3-GO-TiO2 composite with high visible-light-driven photocatalytic activity on degradation of organic dyes, Chemical Physics, 539 (2020) 110950.

[106] M. Abd Mutalib, M. Rahman, M. Othman, A. Ismail, J. Jaafar, Scanning electron microscopy (SEM) and energy-dispersive X-ray (EDX) spectroscopy, Membrane characterization, Elsevier2017, pp. 161-179.

[107] R.K. Mishra, A.K. Zachariah, S. Thomas, Energy-dispersive X-ray spectroscopy techniques for nanomaterial, Microscopy Methods in Nanomaterials Characterization, Elsevier2017, pp. 383-405.

[108] J.R. Lakkakula, T. Matshaya, R.W.M. Krause, Cationic cyclodextrin/alginate chitosan nanoflowers as 5-fluorouracil drug delivery system, Materials Science and Engineering: C, 70 (2017) 169-177.

[109] A. Khan, U. Alam, W. Raza, D. Bahnemann, M. Muneer, One-pot, self-assembled hydrothermal synthesis of 3D flower-like CuS/g-C3N4 composite with enhanced photocatalytic activity under visible-light irradiation, Journal of Physics and Chemistry of Solids, 115 (2018) 59-68.

[110] Y. Duan, X. Li, K. Lv, L. Zhao, Y. Liu, Flower-like g-C3N4 assembly from holy nanosheets with nitrogen vacancies for efficient NO abatement, Applied Surface Science, 492 (2019) 166-176.

[111] D.M. Hercules, Electron spectroscopy: Applications for chemical analysis, Journal of Chemical Education, 81 (2004) 1751.

[112] P. Claesson, A. van der Wal, A. Fogden, New techniques for optimization of particulate cleaning, (2007).

[113] H. Konno, X-ray photoelectron spectroscopy, Materials science and engineering of carbon, Elsevier2016, pp. 153-171.

[114] M. Pazoki, A. Hagfeldt, T. Edvinsson, Characterization Techniques for Perovskite Solar Cell Materials, Elsevier2019.

[115] J. Roberts, A. Power, J. Chapman, S. Chandra, D. Cozzolino, The use of UV-Vis spectroscopy in bioprocess and fermentation monitoring, Fermentation, 4 (2018) 18.

[116] G. George, R. Wilson, J. Joy, Ultraviolet Spectroscopy: A Facile Approach for the Characterization of Nanomaterials, Spectroscopic Methods for Nanomaterials Characterization, Elsevier2017, pp. 55-72.

[117] G. Verma, M. Mishra, Development and optimization of UV-Vis spectroscopy-a review, World Journal of Pharmaceutical Research, 7 (2018) 1170-1180.

[118] A.M. Mohammed, UV-Visible spectrophotometric method and validation of organic compounds, European Journal of Engineering and Technology Research, 3 (2018) 8-11.

[119] J. Njuguna, O.A. Vanli, R. Liang, A review of spectral methods for dispersion characterization of carbon nanotubes in aqueous suspensions, Journal of Spectroscopy, 2015 (2015).

[120] N.M. Aljamali, Review in (NMR and UV-Vis) spectra, International Journal of Medical Research and Pharmaceutical Sciences, 2 (2015) 28-36.

[121] S. Paul, Nanomaterials synthesis by electrodeposition techniques for high-energetic electrodes in fuel cell, Nanomaterials and Energy, 4 (2015) 80-89.

[122] X. Lu, Y. Lin, H. Dong, W. Dai, X. Chen, X. Qu, X. Zhang, One-step hydrothermal fabrication of three-dimensional MoS 2 nanoflower using polypyrrole as template for efficient hydrogen evolution reaction, Scientific Reports, 7 (2017) 1-8.

[123] B. Ma, P.-Y. Guan, Q.-Y. Li, M. Zhang, S.-Q. Zang, MOF-derived flower-like MoS2@ TiO2 nanohybrids with enhanced activity for hydrogen evolution, ACS applied materials & interfaces, 8 (2016) 26794-26800.

[124] X. Liu, J. Zhao, Y. Cao, W. Li, Y. Sun, J. Lu, Y. Men, J. Hu, Facile synthesis of 3D flower-like porous NiO architectures with an excellent capacitance performance, Rsc Advances, 5 (2015) 47506-47510.

[125] R. Bariki, D. Majhi, K. Das, A. Behera, B. Mishra, Facile synthesis and photocatalytic efficacy of UiO-66/CdIn2S4 nanocomposites with flowerlike 3D-microspheres towards aqueous phase decontamination of triclosan and H2 evolution, Applied Catalysis B: Environmental, 270 (2020) 118882.

[126] A. Cheah, W. Chiu, P. Khiew, H. Nakajima, T. Saisopa, P. Songsiririthigul, S. Radiman, M. Hamid, Facile synthesis of a Ag/MoS 2 nanocomposite photocatalyst for enhanced visible-light driven hydrogen gas evolution, Catalysis Science & Technology, 5 (2015) 4133-4143.

[127] K. Chen, L. Ma, J.-H. Wang, Z.-Q. Cheng, D.-J. Yang, Y.-Y. Li, S.-J. Ding, L. Zhou, Q.-Q. Wang, Integrating metallic nanoparticles of Au and Pt with MoS 2–CdS hybrids for high-efficient photocatalytic hydrogen generation via plasmon-induced electron and energy transfer, RSC advances, 7 (2017) 26097-26103.

[128] T. Han, Y. Chen, G. Tian, W. Zhou, Y. Xiao, J. Li, H. Fu, Hydrogenated TiO 2/SrTiO 3 porous microspheres with tunable band structure for solar-light photocatalytic H 2 and O 2 evolution, Science China Materials, 59 (2016) 1003-1016.

[129] K. Nadeem Riaz, N. Yousaf, M. Bilal Tahir, Z. Israr, T. Iqbal, Facile hydrothermal synthesis of 3D flower-like La-MoS2 nanostructure for photocatalytic hydrogen energy production, International Journal of Energy Research, 43 (2019) 491-499.

[130] M.K. Gnanamani, G. Jacobs, H.H. Hamdeh, W.D. Shafer, F. Liu, S.D. Hopps, G.A. Thomas, B.H. Davis, Hydrogenation of carbon dioxide over Co–Fe bimetallic catalysts, Acs Catalysis, 6 (2016) 913-927.

[131] Z. Jiang, T. Xiao, V. Kuznetsov, á & Edwards, PP Turning carbon dioxide into fuel, Phil. Trans. R. Soc. A, 368 (2010) 3343-3364.

[132] J. Schneidewind, R. Adam, W. Baumann, R. Jackstell, M. Beller, Low-temperature hydrogenation of carbon dioxide to methanol with a homogeneous cobalt catalyst, Angewandte Chemie International Edition, 56 (2017) 1890-1893.

[133] W. Wang, S. Wang, X. Ma, J. Gong, Recent advances in catalytic hydrogenation of carbon dioxide, Chemical Society Reviews, 40 (2011) 3703-3727.

[134] S. Michailos, S. McCord, V. Sick, G. Stokes, P. Styring, Dimethyl ether synthesis via captured CO2 hydrogenation within the power to liquids concept: A techno-economic assessment, Energy Conversion and Management, 184 (2019) 262-276.

[135] L. Wang, E. Guan, Y. Wang, L. Wang, Z. Gong, Y. Cui, X. Meng, B.C. Gates, F.-S. Xiao, Silica accelerates the selective hydrogenation of CO 2 to methanol on cobalt catalysts, Nature Communications, 11 (2020) 1-9.

[136] L. Chen, L. Zhang, S. Xia, F. Sun, Entropy generation minimization for CO2 hydrogenation to light olefins, Energy, 147 (2018) 187-196.

[137] B. Hu, S. Frueh, H.F. Garces, L. Zhang, M. Aindow, C. Brooks, E. Kreidler, S.L. Suib, Selective hydrogenation of CO2 and CO to useful light olefins over octahedral molecular sieve manganese oxide supported iron catalysts, Applied Catalysis B: Environmental, 132 (2013) 54-61.

[138] S. Hu, M. Liu, F. Ding, C. Song, G. Zhang, X. Guo, Hydrothermally stable MOFs for CO2 hydrogenation over iron-based catalyst to light olefins, Journal of CO2 Utilization, 15 (2016) 89-95.

[139] J. Zhang, S. Lu, X. Su, S. Fan, Q. Ma, T. Zhao, Selective formation of light olefins from CO2 hydrogenation over Fe–Zn–K catalysts, Journal of CO2 Utilization, 12 (2015) 95-100.

[140] H. Bahruji, R.D. Armstrong, J. Ruiz Esquius, W. Jones, M. Bowker, G.J. Hutchings, Hydrogenation of CO2 to dimethyl ether over Brønsted acidic PdZn catalysts, Industrial & Engineering Chemistry Research, 57 (2018) 6821-6829.

[141] G. Shi, L. Yu, X. Ba, X. Zhang, J. Zhou, Y. Yu, Copper nanoparticle interspersed MoS 2 nanoflowers with enhanced efficiency for CO 2 electrochemical reduction to fuel, Dalton Transactions, 46 (2017) 10569-10577.

[142] S. Gao, Y. Lin, X. Jiao, Y. Sun, Q. Luo, W. Zhang, D. Li, J. Yang, Y. Xie, Partially oxidized atomic cobalt layers for carbon dioxide electroreduction to liquid fuel, Nature, 529 (2016) 68-71.

[143] S. Gao, X. Jiao, Z. Sun, W. Zhang, Y. Sun, C. Wang, Q. Hu, X. Zu, F. Yang, S. Yang, Ultrathin Co3O4 layers realizing optimized CO2 electroreduction to formate, Angewandte Chemie International Edition, 55 (2016) 698-702.

[144] J. Ma, W. Ren, J. Zhao, H. Yang, Growth of TiO2 nanoflowers photoanode for dye-sensitized solar cells, Journal of Alloys and Compounds, 692 (2017) 1004-1009.

[145] J.-N. Zheng, L.-L. He, C. Chen, A.-J. Wang, K.-F. Ma, J.-J. Feng, One-pot synthesis of platinum3cobalt nanoflowers with enhanced oxygen reduction and methanol oxidation, Journal of Power Sources, 268 (2014) 744-751.

[146] R. Miao, W. Zeng, Q. Gao, Hydrothermal synthesis of novel NiO nanoflowers assisted with CTAB and SDS, respectively, and their gas-sensing properties, Materials Letters, 186 (2017) 175-177.

[147] D.J. Yang, Z.F. Zheng, H.Y. Zhu, H.W. Liu, X.P. Gao, Titanate nanofibers as intelligent absorbents for the removal of radioactive ions from water, Advanced Materials, 20 (2008) 2777-2781.

[148] J. Huang, Y. Cao, Z. Deng, H. Tong, Formation of titanate nanostructures under different NaOH concentration and their application in wastewater treatment, Journal of Solid State Chemistry, 184 (2011) 712-719.

[149] S. Sharma, S. Basu, Fabrication of centimeter-sized Sb2S3/SiO2 monolithic mimosa pudica nanoflowers for remediation of hazardous pollutants from industrial wastewater, Journal of Cleaner Production, 280 (2021) 124525.

[150] J. Huang, Y. Cao, Z. Liu, Z. Deng, F. Tang, W. Wang, Efficient removal of heavy metal ions from water system by titanate nanoflowers, Chemical Engineering Journal, 180 (2012) 75-80.

[151] S. Tangsir, L.D. Hafshejani, A. Lähde, M. Maljanen, A. Hooshmand, A.A. Naseri, H. Moazed, J. Jokiniemi, A. Bhatnagar, Water defluoridation using Al2O3 nanoparticles synthesized by flame spray pyrolysis (FSP) method, Chemical Engineering Journal, 288 (2016) 198-206.

[152] K. Vaaramaa, J. Lehto, Removal of metals and anions from drinking water by ion exchange, Desalination, 155 (2003) 157-170.

[153] T. Robinson, G. McMullan, R. Marchant, P. Nigam, Remediation of dyes in textile effluent: a critical review on current treatment technologies with a proposed alternative, Bioresource technology, 77 (2001) 247-255.

[154] B. Zhao, Y. Shang, W. Xiao, C. Dou, R. Han, Adsorption of Congo red from solution using cationic surfactant modified wheat straw in column model, Journal of Environmental Chemical Engineering, 2 (2014) 40-45.

[155] C. Santhosh, V. Velmurugan, G. Jacob, S.K. Jeong, A.N. Grace, A. Bhatnagar, Role of nanomaterials in water treatment applications: a review, Chemical Engineering Journal, 306 (2016) 1116-1137.

[156] E. Ayranci, O. Duman, In-situ UV-visible spectroscopic study on the adsorption of some dyes onto activated carbon cloth, Separation Science and Technology, 44 (2009) 3735-3752.

[157] E. Ayranci, O. Duman, Structural effects on the interactions of benzene and naphthalene sulfonates with activated carbon cloth during adsorption from aqueous solutions, Chemical Engineering Journal, 156 (2010) 70-76.

[158] P.S. Chauhan, R. Kant, A. Rai, A. Gupta, S. Bhattacharya, Facile synthesis of ZnO/GO nanoflowers over Si substrate for improved photocatalytic decolorization of MB dye and industrial wastewater under solar irradiation, Materials Science in Semiconductor Processing, 89 (2019) 6-17.

[159] P.S. Chauhan, A. Rai, A. Gupta, S. Bhattacharya, Enhanced photocatalytic performance of vertically grown ZnO nanorods decorated with metals (Al, Ag, Au, and Au–Pd) for degradation of industrial dye, Materials Research Express, 4 (2017) 055004.

[160] M. Kafil, B. Nasab, H. Moazed, J. Jokiniemi, A. Laehde, A. Bhatnagar, Efficient removal of azo dyes from water with chitosan/carbon nanoflower as a novel nanocomposite synthesized by pyrolysis technique, Desalin. Water Treat, 142 (2019) 308-320.

[161] N. Nandhini, S. Rajeshkumar, S. Mythili, The possible mechanism of eco-friendly synthesized nanoparticles on hazardous dyes degradation, Biocatalysis and Agricultural Biotechnology, 19 (2019) 101138.

[162] M. Tsuboy, J. Angeli, M. Mantovani, S. Knasmüller, G. Umbuzeiro, L. Ribeiro, Genotoxic, mutagenic and cytotoxic effects of the commercial dye CI Disperse Blue 291 in the human hepatic cell line HepG2, Toxicology in vitro, 21 (2007) 1650-1655.

[163] R.L. Singh, P.K. Singh, R.P. Singh, Enzymatic decolorization and degradation of

azo dyes–A review, International Biodeterioration & Biodegradation, 104 (2015) 21-31.

[164] H. Yemendzhiev, Z. Alexieva, A. Krastanov, Decolorization of synthetic dye reactive blue 4 by mycelial culture of white-rot fungi Trametes versicolor 1, Biotechnology & Biotechnological Equipment, 23 (2009) 1337-1339.

[165] S.S. Maurya, S.S. Nadar, V.K. Rathod, Dual activity of laccase-lysine hybrid organic–inorganic nanoflowers for dye decolourization, Environmental Technology & Innovation, 19 (2020) 100798.

[166] C. Chae, S. Jeong, 3D Flower-like Tin Monosulfide/Carbon Nanocomposite Anodes for Sodium-Ion Batteries, Nanomaterials, 12 (2022) 1351.

[167] F. Liang, Z. Zou, S. Zhong, S. Zhang, M. Chen, F. Yu, S. Jia, J. Nong, Metal ions and 3D microstructure engineering enable V2O5·4VO2 enhanced lithium storage, Electrochimica Acta, 470 (2023) 143299.

[168] Y. Liu, R. Wang, N. Huang, Y. Guan, M. Yang, J. Yang, S. Wang, Y. Zhao, B. Jiang, H. Wang, A constructed 3D porous hierarchical micro-flower WO 3/CdS S-scheme heterojunction for boosting photocatalytic H 2 O 2 production and photoelectrochemical cell performance, Journal of Materials Chemistry A, 13 (2025) 14161-14171.

[169] J. Deng, M. Li, Y. Wang, Biomass-derived carbon: synthesis and applications in energy storage and conversion, Green chemistry, 18 (2016) 4824-4854.

[170] K. She, Y. Huang, W. Fan, M. Yu, J. Zhang, C. Chen, 3D flower-like hollow MXene@ MoS2 heterostructure for fast sodium storage, Journal of Colloid and Interface Science, 656 (2024) 270-279.

[171] S. Suresh, A.A. Kumar, S.A. Deshmukh, S. Ravichandran, S. Rafi, P.H. Prasad, 3D Flower-like Composites in Energy Storage and Photocatalytic Applications: A Review, Asian Journal of Chemistry, 36 (2024) 281-293.

[172] P. Rosaiah, J. Zhu, O. Hussain, Y. Qiu, Facile and cost-effective synthesis of flower-like RGO/Fe 3 O 4 nanocomposites with ultra-long cycling stability for supercapacitors, Ionics, 25 (2019) 655-664.

[173] R. Madhuvilakku, S. Alagar, R. Mariappan, S. Piraman, Green one-pot synthesis of flowers-like Fe3O4/rGO hybrid nanocomposites for effective electrochemical detection of riboflavin and low-cost supercapacitor applications, Sensors and Actuators B: Chemical, 253 (2017) 879-892.

[174] Z. Ai, Z. Hu, Y. Liu, M. Fan, P. Liu, Novel 3D flower-like CoNi 2 S 4/carbon nanotube composites as high-performance electrode materials for supercapacitors, New Journal of Chemistry, 40 (2016) 340-347.

[175] M. Li, N. Yu, L. Xu, W. Wang, F. Wei, J. Qi, Y. Sui, Controllable synthesis of flower-like hierarchical CuCo2S4 nanostructure arrays for high-performance hybrid supercapacitors, Metals, 14 (2024) 145.

[176] C.V. Gopi, M. Venkata-Haritha, S.-K. Kim, K. Prabakar, H.-J. Kim, Flower-like ZnO@ MnCo 2 O 4 nanosheet structures on nickel foam as novel electrode material for high-performance supercapacitors, RSC advances, 6 (2016) 102961-102967.

[177] P. Breeze, Power system energy storage technologies, Academic Press2018.

[178] D. Larcher, J.-M. Tarascon, Towards greener and more sustainable batteries for electrical energy storage, Nature Chemistry, 7 (2015) 19-29.

[179] H. Wang, A.L. Rogach, Hierarchical SnO2 nanostructures: recent advances in design, synthesis, and applications, Chemistry of Materials, 26 (2014) 123-133.

[180] J.B. Goodenough, K.-S. Park, The Li-ion rechargeable battery: a perspective, Journal of the American Chemical Society, 135 (2013) 1167-1176.

[181] S. Goriparti, E. Miele, F. De Angelis, E. Di Fabrizio, R.P. Zaccaria, C. Capiglia, Review on recent progress of nanostructured anode materials for Li-ion batteries, Journal of Power Sources, 257 (2014) 421-443.

[182] X. Li, L. Fan, X. Li, H. Shan, C. Chen, B. Yan, D. Xiong, D. Li, Enhanced anode performance of flower-like NiO/RGO nanocomposites for lithium-ion batteries, Materials Chemistry and Physics, 217 (2018) 547-552.

[183] W. Cao, W. Wang, H. Shi, J. Wang, M. Cao, Y. Liang, M. Zhu, Hierarchical three-dimensional flower-like Co 3 O 4 architectures with a mesocrystal structure as high capacity anode materials for long-lived lithium-ion batteries, Nano Research, 11 (2018) 1437-1446.

[184] P.M. Ette, A. Chithambararaj, A. Prakash, K. Ramesha, MoS2 nanoflower-derived interconnected CoMoO4 nanoarchitectures as a stable and high rate performing anode for lithium-ion battery applications, ACS applied materials & interfaces, 12 (2020) 11511-11521.